

Neural Tangent Kernel Maximum Mean Discrepancy

Xiuyuan Cheng* Yao Xie†

Abstract

We present a novel neural network Maximum Mean Discrepancy (MMD) statistic by identifying a new connection between neural tangent kernel (NTK) and MMD. This connection enables us to develop a computationally efficient and memory-efficient approach to compute the MMD statistic and perform NTK based two-sample tests towards addressing the long-standing challenge of memory and computational complexity of the MMD statistic, which is essential for online implementation to assimilating new samples. Theoretically, such a connection allows us to understand the NTK test statistic properties, such as the Type-I error and testing power for performing the two-sample test, by adapting existing theories for kernel MMD. Numerical experiments on synthetic and real-world datasets validate the theory and demonstrate the effectiveness of the proposed NTK-MMD statistic.

1 Introduction

Maximum Mean Discrepancy (MMD) statistic is a popular method in machine learning and statistics. In particular, kernel MMD [2, 23] has been applied to evaluating and training neural network generative models [34, 44, 31, 3, 30]. Though a widely used non-parametric test [23], kernel MMD encounters several challenges in practice. The roadblocks for large-scale implementation of kernel MMD involve heavy memory requirement (due to the computation and storage of the Gram matrix, which grows quadratically with the data size) and the choice of a good kernel function for high dimensional data. While Gaussian RBF kernel was shown to provide a metric between pairs of probability distributions with infinite data samples, applying isotropic Gaussian kernel to data in applications, such as image data and discrete events data, may invoke issues in terms of kernel expressiveness [25, 29, 36] and sampling complexity [38].

A potential path forward in developing more computationally and memory-efficient testing statistics is to leverage deep neural networks' representation and optimization advantage. For example, the idea of training a classification neural network for testing problems has been revisited recently in [37, 10], and the connection between classification and two-sample testing dates back to earlier works [19, 43, 40]. However, in applying deep models to testing problems, the test consistency analysis is usually incomplete due to the lack of optimization guarantee of the trained network. For one thing, assuming perfect training of a deep network to achieve global minimizer is too strong an assumption to fulfill in practice.

A recent focus of neural network optimization research is the so-called lazy training regime of over-parametrized neural networks [13], where the neural network training dynamics exhibit certain linearized property and provable learning guarantee can be obtained [33, 17, 15, 1]. In this regime, the training time is sufficiently short, and networks are sufficiently parametrized such that network parameters stay close to the randomized initial values over the training process. In particular, the Neural Tangent Kernel (NTK) theory, as firstly described by [28], shows that the network optimization can be well approximated by the Reproducing Kernel Hilbert Space (RKHS) formulation. The NTK theory has been developed for general neural network architectures, including deep fully connected networks [48], convolutional networks [6, 35],

*Department of Mathematics, Duke University. Email: xiuyuan.cheng@duke.edu

†H. Milton Stewart School of Industrial and Systems Engineering, Georgia Institute of Technology. Email: yao.xie@isye.gatech.edu.

graph neural networks [16], and residual networks [45, 27, 7]. The RKHS approach by NTK has been shown theoretically and empirically to characterize the wide neural network training dynamic in the early stage.

The current work stems from a simple observation that short-time training of a network is approximately equivalent to computing the *witness function* of a kernel MMD with NTK at time zero, when the training objective equals the difference between sample averages of the network function on two samples. The proposed test statistic, called NTK-MMD, approximates the classical kernel MMD with NTK, and the error at training time t can be bounded to be $O(t)$ under the linearization of the NTK theory. The theoretical benefit of translating the network-based statistic into a kernel MMD is that the testing power of the latter can be analyzed based on previous works. Algorithm-wise, the network-based test statistic can be computed on the fly: thanks to the form of linear accumulation of the training objective, the training allows small-batch, e.g., batch size 1 and 1 epoch of training (1 pass of the samples), under the NTK approximation. To calibrate the testing threshold needed to prevent false alarm, we introduce an asymmetric MMD using training-testing split and theoretically prove the testing power where the threshold is estimated from bootstrapping on the test split only and thus avoids retraining network.

Our main contributions include the following: (i) We introduce a neural network-based test statistic called NTK-MMD, which can be computed by a short-time training of a neural network, particularly online learning using one-pass of the training samples and batch size one. The NTK approximation error of the MMD statistic is shown to be linear in training time, which leads to the construction of the NTK-MMD test statistic; (ii) We characterize the statistical properties of the NTK-MMD, including the Type-I error and the testing power, which establish the conditions under which the test is powerful; we further introduce a data split scheme such that the test threshold can be estimated without network retraining with provable testing power guarantee; (iii) The efficiency of the proposed NTK-MMD test is demonstrated on simulated and real-world datasets.

At the same time, we are aware of the limitations of NTK in explaining deep network optimization, expressiveness power, and so on. We discuss limitations and extensions in the last section. In particular, this paper focuses on demonstrating the power of NTK-MMD statistics for the two-sample test, while the proposed computationally and memory-efficient NTK-MMD statistics can also be used for other applications of MMD statistics other than the two-sample testing problem [24].

2 Method

2.1 Preliminary: Kernel MMD

We start by reviewing a few preliminaries. Consider data in $\mathcal{X} \subset \mathbb{R}^d$, sampled from two unknown distributions with densities p and q . Given two data sets

$$X = \{x_i \sim p, \text{ i.i.d.}, i = 1, \dots, n_X\}, \quad Y = \{y_j \sim q, \text{ i.i.d.}, j = 1, \dots, n_Y\}, \quad (1)$$

we would like to test whether or not they follow the same distribution. This is equivalent to perform the following hypothesis test $H_0 : p = q$ versus $H_1 : p \neq q$. The classical kernel MMD considers test functions in the RKHS of positive semi-definite kernel $K(x, y)$, which can be, for instance, the Gaussian RBF kernel. The (squared and biased) empirical kernel MMD statistic is given by [23]:

$$\text{MMD}_K^2 = \int_{\mathcal{X}} \int_{\mathcal{X}} K(x, y) (\hat{p} - \hat{q})(x) (\hat{p} - \hat{q})(y) dx dy, \quad \hat{p} := \frac{1}{n_X} \sum_{i=1}^{n_X} \delta_{x_i}, \quad \hat{q} := \frac{1}{n_Y} \sum_{i=1}^{n_Y} \delta_{y_i}. \quad (2)$$

The null hypothesis is rejected if $\text{MMD}_K^2 > t_{\text{thres}}$, where t_{thres} is the user-specified test threshold (usually, chosen to control the false alarm up to certain level). The (empirical) *witness function* of the MMD statistic, $\hat{w}(x) = \int_{\mathcal{X}} K(x, y) (\hat{p} - \hat{q})(y) dy$, indicates where the two densities differ. The Type-I error of the

test is defined as $\mathbb{P}[\text{MMD}_K^2 > t_{\text{thres}}]$ under H_0 , and the Type-II error as $\mathbb{P}[\text{MMD}_K^2 \leq t_{\text{thres}}]$ under H_1 ; the power is defined as one minus the Type-II error. For an alternative distribution q of p , the test errors depend on q , the sample sizes n_X and n_Y , as well as the kernel function $K(x, y)$. Theoretically, the test power of kernel MMD has been analyzed in [23], investigated for high dimensional Gaussian data in [38], and for manifold data in [12].

2.2 NTK-MMD statistic

As the proposed NTK-MMD framework can be used on different network architectures, we write the neural network mapping abstractly as $f(x; \theta)$, which maps from input $x \in \mathcal{X}$ to \mathbb{R} , and θ is the network parameters. Use $X \cup Y$ as the training dataset, and let \hat{p} and \hat{q} be as in (2), we choose a particular training objective function as

$$\hat{L}(\theta) = - \int_{\mathcal{X}} f(x; \theta)(\hat{p} - \hat{q})(x) dx = - \frac{1}{n_X} \sum_{i=1}^{n_X} f(x_i; \theta) + \frac{1}{n_Y} \sum_{i=1}^{n_Y} f(y_i; \theta) \quad (3)$$

The choice of this objective function is critical in establishing the connection between NTK and MMD. Optimizing this objective will lead to divergence of the network function if we train for a long time. However, if the training is only for a short time, the network function remains finite. Here we mainly focus on short-time training of the network, and particularly the online training setting where the number of epochs is 1, that is, only 1-pass of the training samples is used. We will also show that the method allows using minimal batch size for online learning without affecting the NTK approximation of the MMD statistic, c.f. Remark 2.2.

Following the convention in NTK literature, below we formulate in terms of continuous-time Gradient Descent (GD) dynamic of the network training. The extension to discrete-time Stochastic Gradient Descent (SGD) holds with a small learning rate (Remark 2.2). The network parameter $\theta(t)$ evolves according to $\dot{\theta}(t) = -\partial \hat{L} / \partial \theta$, and we define $u(x, t) := f(x, \theta(t))$, which is the network mapping function at time t . Suppose the network is trained for a short time $t > 0$, we define

$$\hat{g}(x) := \frac{1}{t}(u(x, t) - u(x, 0)), \quad (4)$$

and the test statistic, which depends on time t , is

$$\hat{T}_{\text{net}}(t) := \int_{\mathcal{X}} \hat{g}(x)(\hat{p} - \hat{q})(x) dx = \frac{1}{t} \left(\hat{L}(\theta(t)) - \hat{L}(\theta(0)) \right). \quad (5)$$

The function \hat{g} is the difference of the network mapping after a short-time training from the initial one, and we call it the *witness function* of network NTK-MMD statistic. As revealed by (5), (without calibrating the test threshold) the test statistics \hat{T}_{net} is nothing but the decrease in the training objective, and comes as a by-product of network training at no additional computational cost. We show in next subsection that at small t , the statistic $\hat{T}_{\text{net}}(t)$ provably approximates the classical MMD statistic with the NTK, i.e. $\hat{T}_{\text{NTK}} = \text{MMD}_K^2(X, Y)$ where K is the NTK at time $t = 0$ as in (8). Algorithmically, we will perform two-sample test using $\hat{T}_{\text{net}}(t)$ by comparing with a threshold t_{thres} .

2.3 NTK approximation of MMD statistic

In the continuous-time training dynamic of the network, we consider the NTK [28] kernel function defined for $t > 0$ as

$$\hat{K}_t(x, x') := \langle \nabla_{\theta} f(x; \theta(t)), \nabla_{\theta} f(x'; \theta(t)) \rangle. \quad (6)$$

The following lemma follows directly by construction, and the proof is in Appendix A.1.

Lemma 2.1. *The network function $u(x, t)$ satisfies that for $t > 0$,*

$$u(x, t) - u(x, 0) = \int_0^t \int_{\mathcal{X}} \hat{K}_s(x, x')(\hat{p} - \hat{q})(x') dx' ds. \quad (7)$$

It has been shown (in [6, 5, 13], among others) that for the short-time training (lazy training regime), the kernel (6) can be well-approximated by the kernel at time $t = 0$, namely

$$K_0(x, x') := \langle \nabla_{\theta} f(x; \theta(0)), \nabla_{\theta} f(x'; \theta(0)) \rangle, \quad (8)$$

which is only determined by the network weight initialization $\theta(0)$. Assuming $K_0 \approx \hat{K}_t$ in Lemma 2.1, the proposed test statistic $\hat{T}_{\text{net}}(t)$ as in (5) can be viewed as

$$\hat{T}_{\text{net}}(t) \approx \hat{T}_{\text{NTK}} := \int_{\mathcal{X}} \int_{\mathcal{X}} K_0(x, x')(\hat{p} - \hat{q})(x)(\hat{p} - \hat{q})(x') dx dx', \quad (9)$$

which is the kernel MMD statistic with NTK. (See Remark A.1 for a discussion on biased/unbiased MMD estimator.) In below, we show in Proposition 2.1 that the approximation $\hat{T}_{\text{net}} \approx \hat{T}_{\text{NTK}}$ has $O(t)$ error, and we experimentally verify the similarity of the two statistics in Subsection 4.2. Throughout the paper, we compute \hat{T}_{net} by neural network training, and we call \hat{T}_{NTK} the *exact* NTK-MMD which is for theoretical analysis. The theoretical benefit of translating \hat{T}_{net} into \hat{T}_{NTK} lies in that testing power analysis of \hat{T}_{NTK} follows existing methods which is detailed in Section 3.

Suppose neural network parameter θ is in \mathbb{R}^M and $\theta \in \Theta$, where Θ is a domain in \mathbb{R}^M which contains the Euclidean ball $B(\theta(0), r_0)$, where we assume r_0 is an $O(1)$ constant. For vector valued function $g : (\mathcal{X}, \Theta) \rightarrow \mathbb{R}^d$ and $U \subset \Theta$, we denote the infinity norm as $\|g\|_{\mathcal{X}, U} := \sup_{x \in \mathcal{X}, \theta \in U} \|g(x, \theta)\|$. When g maps to a matrix, the notation denotes (the infinity norm over $(\mathcal{X} \times U)$ of) the operator norm. The test statistic approximation error in Proposition 2.1 directly follows the following lemma concerning the uniform approximation of the kernels. All proofs in Appendix A.1.

Lemma 2.2 (NTK kernel approximation). *Suppose f is C^2 on (\mathcal{X}, Θ) and $\|\nabla_{\theta} f\|_{\mathcal{X}, \Theta} \leq L_f$ for some positive constant L_f . Then for any $0 < r < r_0$, when $0 < t < t_{f,r} := r/(2L_f)$,*

- (1) $\theta(t)$ stays inside the Euclidean ball $B_r := B(\theta(0), r)$.
- (2) Define $C_{f,r} := 4\|D_{\theta}^2 f\|_{\mathcal{X}, B_r} \|\nabla_{\theta} f\|_{\mathcal{X}, B_r}^2$, we have that

$$\sup_{x, x' \in \mathcal{X}} |\hat{K}_t(x, x') - K_0(x, x')| \leq C_{f,r} t. \quad (10)$$

Remark 2.1 (Boundedness of $\|\nabla_{\theta} f\|_{\mathcal{X}, \Theta}$). When p are unbounded density (gaussian), and activation function f is relu or softplus, the uniform boundedness of $\|\nabla_{\theta} f\|_{\mathcal{X}, \Theta}$ may fail. However, for sub-exponential densities, apply standard truncation argument, and when we restrict to compactly supported distributions. In practice, we standardize the data to be on a compact domain in \mathbb{R}^d .

Proposition 2.1 (Test statistic approximation). *The condition on $f(x, \theta)$ is the same as in Lemma 2.2, and for $0 < r < r_0$, the constants $t_{f,r}$ and $C_{f,r}$ are as therein. Then, when $0 < t < t_{f,r}$, we have that*

$$|\hat{T}_{\text{net}}(t) - \hat{T}_{\text{NTK}}| \leq 2C_{f,r} t.$$

Remark 2.2 (SGD and online training). The above error bound analysis based on Taylor expansion can extend to discrete-time GD dynamic by showing that the time discretization introduces higher-order error when t is small. In the SGD setting, e.g., the online learning of 1 epoch, batch size one, and learning rate α , the network parameters are updated after scanning each training sample on the fly. Let θ_k be the network after scanning k many samples, we show in Appendix A.2 that the difference $\|\theta_k - \theta_0\|$ can be bounded by $O(\alpha k/n)$, and the trained network witness function after 1 epoch approximates the witness

function with the zero-time NTK kernel up to an $O(\alpha)$ error. The learning rate α has the role of training time t . The fact that batch size will not affect the NTK approximation of the network training is a result of that the loss (3) is a linear accumulation over samples, which may not hold for other loss types. The compatibility with online learning and training with very small batch size of NTK-MMD statistic makes it convenient for deep network training, especially under memory constraints.

2.4 Computational and memory efficiency

The update of network parameters in NTK-MMD training can be viewed as an implicit computation of the inner-product between high dimensional kernel feature maps $\langle \nabla_{\theta} f(x; \theta(t)), \nabla_{\theta} f(x'; \theta(t)) \rangle$ (by chain rule, c.f. (24) (25) in Appendix A.1). The network witness function \hat{g} defined in (4) is parametrized and stored in trained network parameters. This allows the (approximate) evaluation of kernel on a test sample x' without computing the gradient $\nabla_{\theta} f(x'; \theta)$ explicitly. It also means that the NTK network witness function can be evaluated on any new x' without revisiting the training set. In contrast, traditional kernel MMD computes kernel witness function (defined as $\int K(x, y)(\hat{p} - \hat{q})(y)dy$ [23]) on a new point x' by pairwise computation between x' and samples in datasets X and Y .

NTK-MMD can be computed via batch-size-one training over one-pass of the training set (c.f. Remark 2.2 and experimentally verified in Table A.2). The gradient field evaluation (back propagation) is only conducted on the training set but not the testing test, and the bootstrap calibration of the test threshold can be computed from test set only (c.f. Section 3.2). Thus, by using small learning rate (allowed by floating point precision, c.f. Remark C.1), one can incorporate large number of training samples via more training iterations without worsening the approximation error to exact NTK-MMD, which will improve testing power. This “separation” of training and testing, in memory and computation, of NTK-MMD allows scalable online learning as well as efficient deployment of the network function on potentially large test sets.

3 Theoretical properties of NTK-MMD

In this section, we prove the testing power (at a controlled level) of the NTK-MMD statistic \hat{T}_{NTK} as in (9) with large enough finite samples. We also introduce an asymmetric version of the MMD statistic using training-testing dataset splitting, which enables the bootstrap estimation of the threshold of the test t_{thres} without retraining of the neural network.

3.1 NTK-MMD without data splitting

We write the NTK kernel $K_0(x, x')$ as $K(x, x')$ omitting the $_{NT}$ subscript, and assume that $K(x, x')$ is uniformly bounded, that is, $\sup_{x \in \mathcal{X}} K(x, x) \leq B < \infty$ for some positive constant B . Without loss of generality, we assume that $B = 1$ (because a global constant normalization of the kernel does not change the testing). By that the kernel is PSD, we thus have that

$$\sup_{x', x \in \mathcal{X}} |K(x, x')| \leq 1. \quad (11)$$

We omit the $_{\text{NTK}}$ subscript and denote the MMD statistic (9) as \hat{T} . The corresponding population statistic is the squared MMD of kernel $K(x, y)$

$$\delta_K := \text{MMD}_K^2(p, q) = \int_{\mathcal{X}} \int_{\mathcal{X}} K(x, y)(p - q)(x)(p - q)(y) dx dy. \quad (12)$$

By the uniform boundedness (11), the kernel $K(x, x')$ is in $L^2(\mathcal{X} \times \mathcal{X}, (p+q)(x)(p+q)(x')dx dx')$. We define the squared integrals of the kernel

$$\nu_{pp} := \mathbb{E}_{x \sim p, y \sim p} K(x, y)^2, \quad \nu_{pq} := \mathbb{E}_{x \sim p, y \sim q} K(x, y)^2, \quad \nu_{qq} := \mathbb{E}_{x \sim q, y \sim q} K(x, y)^2. \quad (13)$$

In addition, we assume that as $n := n_X + n_Y$ increases, n_X/n stay bounded and approaches $\rho_X \in (0, 1)$. Equivalently, there is some constant $0 < c < 1$ such that for large enough n ,

$$cn + 1 \leq n_X, n_Y \leq n, \quad i = 1, 2. \quad (14)$$

Without loss of generality, we assume that (14) always holds for the n considered.

Theorem 3.1 (Test power of \hat{T}_{NTK}). *Suppose (11) and (14) hold, and*

- (i) *Under H_1 , $p \neq q$, the squared population kernel MMD δ_K as in (12) is strictly positive,*
- (ii) *The three integrals as in (13), $\nu_{pp}, \nu_{pq}, \nu_{qq}$, are all bounded by a constant $\nu \leq 1$.*

Define $\lambda_1 := \sqrt{8 \log(4/\alpha_{\text{level}})}$, and let the threshold for the test be $t_{\text{thres}} = 4/(cn) + 4\lambda_1 \sqrt{\nu/cn}$. Then, if for some $\lambda_2 > 0$, n is large enough such that

$$n > \frac{1}{c} \max \left\{ \frac{1}{9\nu} \max\{\lambda_1, \lambda_2\}^2, \frac{8}{\delta_K}, \frac{\nu}{\delta_K^2} (8(\lambda_1 + \lambda_2))^2 \right\}, \quad (15)$$

then under H_0 , $\mathbb{P}[\hat{T} > t_{\text{thres}}] \leq \alpha_{\text{level}}$; and under H_1 , $\mathbb{P}[\hat{T} \leq t_{\text{thres}}] \leq 3e^{-\lambda_2^2/8}$.

The proof uses the U-statistic concentration analysis, and is left to Appendix B. As revealed by the proof, the diagonal entries in the kernel matrix contribute to the $O(1/n)$ term, and thus switching from the biased estimator of MMD (9) to the unbiased estimator gives similar theoretical results.

Remark 3.1 (Choice of t_{thres}). The choice of t_{thres} in the above theorem is a theoretical one and may not be optimal, due to the use of concentration inequality and the relaxation of the bounds by using constants ν and c . By definition, the optimal value of t_{thres} is the $(1 - \alpha_{\text{level}})$ -quantile of the distribution of \hat{T} under H_0 . The asymptotic choice may be obtained analytically according to the limiting distribution of the MMD statistic, c.f. Remark B.1. The threshold t_{thres} is also computed by a bootstrap strategy in practice [4] (called “full-bootstrap” in next subsection). The bootstrap approach permutes the labels in data sets X and Y , and since in \hat{T}_{net} the witness function $\hat{g}(x)$ is computed by neural network training, this will incur retraining of the network. A solution to avoid retraining by adopting a test set for bootstrap estimation of t_{thres} is introduced in next subsection.

3.2 Threshold calibration by data splitting

As shown in Theorem 3.1 and Remark 3.1, in the theoretical characterization of test power (at a required test level) the test threshold plays a critical role. In practice, we need a more precise threshold to exactly control the false alarm under the null hypothesis. In this section, we discuss how to set the threshold in two settings: fixed-sample and pilot-data. Nevertheless, we would like to mention that there exist applications where the threshold is not needed, and the symmetric MMD \hat{T}_{NTK} can be used as a measurement of distribution divergence.

Fixed-sample setting. We first consider the setting where we have a fixed number of samples from p and q . To obtain a precise threshold to control the false alarm, we need to split data into two non-overlapping parts: one part for training neural networks (compute the witness function) and one part data for bootstrapping and calibrating the threshold. We want to highlight that here we develop a scheme for threshold calibration such that no re-training of the witness function is necessary.

We randomly split the datasets X and Y into training and testing sets, $X = X_{(1)} \cup X_{(2)}$ and $Y = Y_{(1)} \cup Y_{(2)}$, and compute an asymmetric version of kernel MMD (the subscript a is for “asymmetric”)

$$\hat{T}_a := \int_{\mathcal{X}} \int_{\mathcal{X}} K(x, x') (\hat{p}_{(1)} - \hat{q}_{(1)})(x') (\hat{p}_{(2)} - \hat{q}_{(2)})(x) dx dx', \quad (16)$$

where $\hat{p}_{(i)}$ and $\hat{q}_{(i)}$ are the empirical measures of datasets $X_{(i)}$ and $Y_{(i)}$ respectively, $i = 1, 2$. Define $n_{X,(i)} = |X_{(i)}|$ and $n_{Y,(i)} = |Y_{(i)}|$, $i = 1, 2$. Similarly as in Section 2, the MMD statistic (16) with $K(x, y) = K_0(x, y)$, the zero-time NTK, can be approximated by

$$\hat{T}_{a,\text{net}}(t) = \int_{\mathcal{X}} \hat{g}_{(1)}(x)(\hat{p}_{(2)} - \hat{q}_{(2)})(x)dx, \quad \hat{g}_{(1)}(x) = \frac{1}{t}(\hat{u}(x, t) - \hat{u}(x, 0)), \quad (17)$$

for a small time t , where $\hat{u}(x, t)$ is the network function trained by minimizing $\hat{L}(\theta) := -\int_{\mathcal{X}} f(x; \theta)(\hat{p}_{(1)} - \hat{q}_{(1)})(x)dx$ on the training set $\mathcal{D}_{tr} = \{X^{(1)}, Y^{(1)}\}$ with binary labels $\{1, 2\}$. Same as in Lemma 2.2 Proposition 2.1, the difference $|\hat{T}_a - \hat{T}_{a,\text{net}}(t)|$ can be bounded to be $O(t)$. We theoretically analyze the testing power of \hat{T}_a where $K(x, y) = K_0(x, y)$ in below.

The benefit of splitting the test set lies in that once the witness function $\hat{g}_{(1)}(x)$ is trained from \mathcal{D}_{tr} , one can do a *test-only bootstrap* which is to compute

$$\hat{T}_{a,\text{null}} = \int_{\mathcal{X}} \hat{g}_{(1)}(x)(\hat{p}'_{(2)} - \hat{q}'_{(2)})(x)dx, \quad (18)$$

where $\hat{p}'_{(2)}$ and $\hat{q}'_{(2)}$ are empirical measure of samples in $\mathcal{D}_{te} = \{X^{(2)}, Y^{(2)}\}$ by randomly permute the $n_{X,(2)} + n_{Y,(2)}$ many binary class labels. Since permuting test labels does not affect $\hat{g}_{(1)}(x)$, the test-only bootstrap does not require retraining of the network. Alternatively, one can permute the binary class labels in both \mathcal{D}_{tr} and \mathcal{D}_{te} , and will require to retain the neural network to obtain the new witness function $\hat{g}_{(1)}$ given the new class labels of \mathcal{D}_{tr} . We call such a bootstrap the *full-bootstrap*. The full-bootstrap can be applied to the symmetric MMD statistic without test set splitting as well, namely the setting of Theorem 3.1, to obtain an estimate of optimal t_{thres} .

We give two theoretical results on the testing power guarantee of the asymmetric NTK MMD statistic (16): For *test-only bootstrap*, Theorem 3.2 proves testing power by restricting to good events over the randomness of \mathcal{D}_{tr} ; For *full bootstrap*, the guarantee is provided in Theorem 3.3, which is the counterpart of Theorem 3.1. All proofs are in Appendix B.

We assume the balance-ness of the two samples as well as the training and testing splitting, that is, $n_{X,(1)}/n_X \rightarrow \rho_{X,(1)}$, $n_{Y,(1)}/n_Y \rightarrow \rho_{Y,(1)}$, $n_X/n \rightarrow \rho_X$, and the three constants are all in $(0, 1)$. With $n = n_X + n_Y$, we assume for constant $0 < c < 1$.

$$c_a n \leq n_{X,(i)}, n_{Y,(i)} \leq n, \quad i = 1, 2. \quad (19)$$

We denote by $\mathbb{P}_{(1)}$ the randomness over \mathcal{D}_{tr} , and $\mathbb{P}_{(2)}$ that over \mathcal{D}_{te} .

Theorem 3.2 (Test power of \hat{T}_a , test-only bootstrap). *Suppose that (11), (19) and the conditions (i) and (ii) in Theorem 3.1 hold, and $0 < \gamma < 1$ is a small number. Define $\lambda_{(2),1} := \sqrt{4 \log(4/\alpha_{\text{level}})}$, $\lambda_{(1)} := \sqrt{4 \log(8/\gamma)}$, and set the threshold as $t_{\text{thres}} = 4(\sqrt{1.1}\lambda_{(2),1} + \lambda_{(1)})\sqrt{\nu/(c_a n)}$. If n is large enough such that $n > (\frac{\lambda_{(1)}}{0.1\nu})^2/(8c_a)$, and for some $\lambda_{(2),2} > 0$,*

$$n > \frac{1}{c_a} \max \left\{ \frac{1}{9\nu} \max\{\lambda_{(1)}, \lambda_{(2),1}, \lambda_{(2),2}\}^2, \frac{16\nu}{\delta_K^2} \left(2\lambda_{(1)} + \sqrt{1.1}(\lambda_{(2),1} + \lambda_{(2),2}) \right)^2 \right\}, \quad (20)$$

then, under both H_0 and H_1 there is a good event over the randomness of \mathcal{D}_{tr} which happens w.p. $\geq 1 - \gamma$, under which, conditioning on \mathcal{D}_{tr} , $\mathbb{P}_{(2)}[\hat{T}_a > t_{\text{thres}}] \leq \alpha_{\text{level}}$ under H_0 , and $\mathbb{P}_{(2)}[\hat{T} \leq t_{\text{thres}}] \leq 4e^{-\lambda_{(2),2}^2/4}$ under H_1 .

Remark 3.2 (Sampling complexity). Compared to the full-bootstrap result Theorem 3.3, the additional requirement on n is that $c_a n$ needs to be greater than $(\lambda_{(1)}/\nu)^2$ up to absolute constant, and thus when $\nu/\delta_K^2 \gg \nu^{-2}$, the (ν/δ_K^2) -term still dominates the needed lower bound of n , same as in Theorems 3.1 and

3.3. (Here we treat $\lambda_{(1)}$, $\lambda_{(2),1}$ and $\lambda_{(2),2}$ as $O(1)$ constants. Because the constant γ controls the good event probability over the randomness of \mathcal{D}_{tr} , thus if γ can be chosen to be of the same order as α_{level} , then $\lambda_{(1)}$ has the same order as $\lambda_{(2),1}$.) The result shows that with test split and test-only bootstrap (avoiding re-training), the test power has the same order of needed sampling complexity, $n \gtrsim \nu/\delta_K^2$, as full bootstrap, with high probability and for large enough n .

Theorem 3.3 (Test power of \hat{T}_a , full bootstrap). *Suppose that (11), (19) and the conditions (i) and (ii) in Theorem 3.1 hold. Define $\lambda_1 := \sqrt{8 \log(4/\alpha_{\text{level}})}$, and let the threshold for the test be $t_{\text{thres}} = 4\lambda_1 \sqrt{\frac{\nu}{c_a n}}$. Then, if for some $\lambda_2 > 0$, n is large enough such that*

$$n > \frac{1}{c_a} \max \left\{ \frac{1}{9\nu} \max\{\lambda_1, \lambda_2\}^2, \frac{\nu}{\delta_K^2} (4(\lambda_1 + \lambda_2))^2 \right\}, \quad (21)$$

then under H_0 , $\mathbb{P}[\hat{T} > t_{\text{thres}}] \leq \alpha_{\text{level}}$; and under H_1 , $\mathbb{P}[\hat{T} \leq t_{\text{thres}}] \leq 4e^{-\lambda_2^2/8}$.

Pilot data setting. This section considers the setting where we may have many samples for one distribution, e.g., the p . For instance, in change-point detection, where we are interested in detecting a shift in the underlying data distribution, there can be a large pool of pilot data before the change happens, collected historically and representing the normal status. We may have fewer data samples for the distribution q . For such a case, we can use data from the reference pool represent distribution p to train the model and calibrate the threshold, e.g., using bootstrap. Since such “training” is done offline, we can afford the higher computational cost associated with training the model multiple times. In short, our strategy is to pre-compute the detector (re-train multiple times) and then use bootstrap to obtain the threshold t_{thres} for detector: (i) compute the symmetric MMD \hat{T}_{NTK} on $\{\hat{p}, \hat{q}\}$, where \hat{q} is the new coming test samples (e.g. in change-point detection), and \hat{p} is from the pool. (ii) pre-compute the symmetric MMD \hat{T}_{null} on $\{\hat{p}_2, \hat{p}'_2\}$ from the pool of samples, with retrain, and obtain the “true” threshold for \hat{T}_{NTK} . Re-training of the network is expensive, but this is pre-computation and not counted in the online computation.

4 Numerical experiments

The section presents several experiments to examine the proposed method and validate the theory. ¹

4.1 Gaussian mean and covariance shifts

Set-up. Consider Gaussian mean shift and covariance shift in \mathbb{R}^{100} , where $n_X = n_Y = 200$; p is the distribution of $\mathcal{N}(0, I_d)$, $d = 100$: (i) Mean-shift: q is the distribution of $\mathcal{N}(\mu, I_d)$, where $\|\mu\|_2 = \delta$ which varies from 0 to 0.8 and (ii) Covariance-shift: q is the distribution of $\mathcal{N}(0, I_d + \rho E)$, where E is an d -by- d all-ones matrix, and ρ changes from 0 to 0.16. We split training and test sets into halves, and compute the asymmetric network approximated NTK MMD statistic $\hat{T}_{a,\text{net}}$ (17), and estimate the test threshold by the quantile of (18); H_0 is rejected if $\hat{T}_{a,\text{net}} > t_{\text{thres}}$. We use a 2-layer network (1 hidden layer) with soft-plus activation. The online training is of 1 epoch (1 pass over the training set) with batch-size = 1. The bootstrap estimate of test threshold uses $n_{\text{boot}} = 400$ permutations. The testing power is approximated by $n_{\text{run}} = 500$ Monte Carlo replicas, and we compare with the benchmarks by (i) Hotelling’s T-test, and (ii) Gaussian kernel MMD test (median distance bandwidth) [23]. The median distance bandwidth is a reasonable choice for detecting high dimensional Gaussian mean shift [38]. Both Gaussian kernel MMD and Hotelling’s Test have access to all the samples $\mathcal{D}_{tr} \cup \mathcal{D}_{te}$. More experimental details are in Appendix C.1.

¹Code available at <https://github.com/xycheng/NTK-MMD/>.

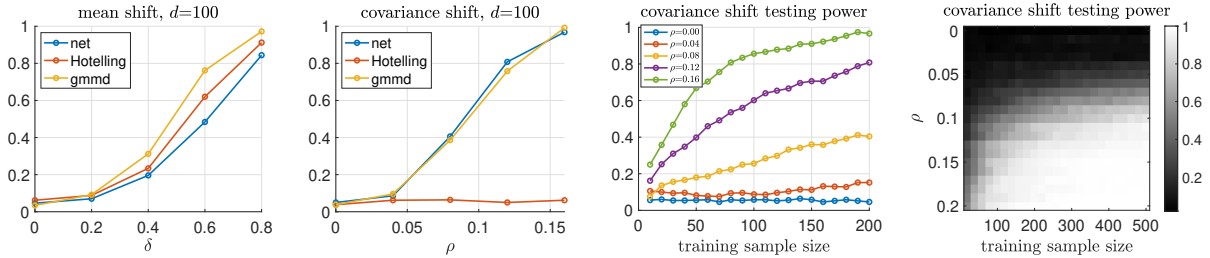


Figure 1: (Left two plots) Estimated testing power on Gaussian mean shift (change size is δ) and Gaussian covariance shift (change size is ρ) in \mathbb{R}^{100} , where datasets X and Y have 200 samples respectively, and the training and testing splitting is half-half, i.e. $n_{tr} = n_{te} = 200$. Test power is estimated from $n_{run} = 500$. (Right two plots) Estimated testing power as a function of the number of samples processed in the 1-pass of the training set (batch size =1) and over varying values of ρ , also plotted as a color field.

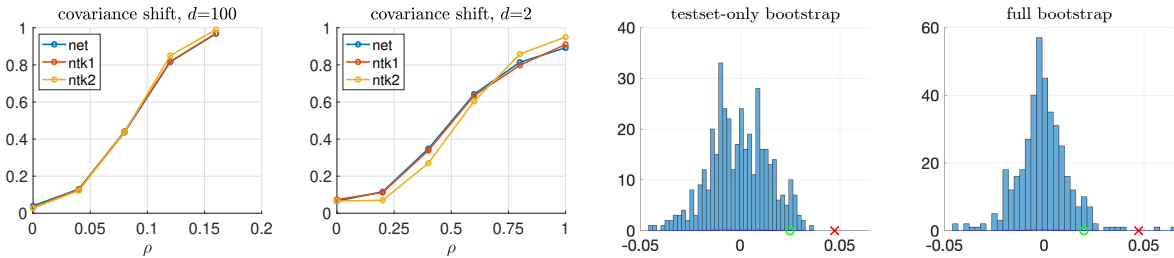


Figure 2: (Left two plots) Estimated testing power from $n_{run} = 500$ of the covariance shift test in Figure 1 in \mathbb{R}^{100} and \mathbb{R}^2 . $n_X = n_Y = 200$, using three statistics: \hat{T}_{net} (net), \hat{T}_{NTK} with test set only bootstrap (ntk1) and with full bootstrap (ntk2) the training and testing splitting is half-half. (Right two plots) Test statistics \hat{T}_a (red cross), the empirical distribution of $\hat{T}_{a, null}$ using the test-only bootstrap and the full bootstrap (blue bars), and the estimated threshold (green circle). Computed from NTK kernel at $t = 0$ and $n_{boot} = 400$.

Results. The results are shown in the left two plots in Figure 1. The NTK MMD test gives comparable but slightly worse power than the other two benchmarks on the mean shift. On the covariance shift test, the network MMD test gives equally good power as the Gaussian MMD. For the Gaussian covariance shift case, we also compute the testing power when only part of the training samples are used in the online training, and the results are shown in the right two plots in Figure 1. Testing power increases as the neural network scans more training samples, and when the covariance shifts are larger the transition takes place with smaller training sample size.

In addition, we show in Appendix C.2 that NTK-MMD gives similar performance with varying network architectures, activation functions (like relu), and SGD configurations, and possibly better testing power with a larger network depth and width (Tables A.1 and A.2). We also compare with linear-time kernel MMD in Appendix C.7. As shown in Table A.3, NTK-MMD outperforms linear-time gMMD as in [23, Section 6], and underperforms the full gMMD which however requires $O(n^2)$ computation and storage.

4.2 Comparison of \hat{T}_{net} and \hat{T}_{NTK}

Set-up. Since we use a 2-layer fully-connected network, the finite-width NTK at $t = 0$ (using initialized neural network parameters) can be analytically computed, which gives an n_{te} -by- n_{tr} asymmetric kernel matrix K . The expression of K and more details are provided in Appendix C.3. This allows computing the exact NTK MMD (16), as well as the (i) full bootstrap and (ii) the test-only bootstrap of the MMD statistic under H_0 by (i) permuting both rows and columns simultaneously and (ii) only permuting rows of the matrix K .

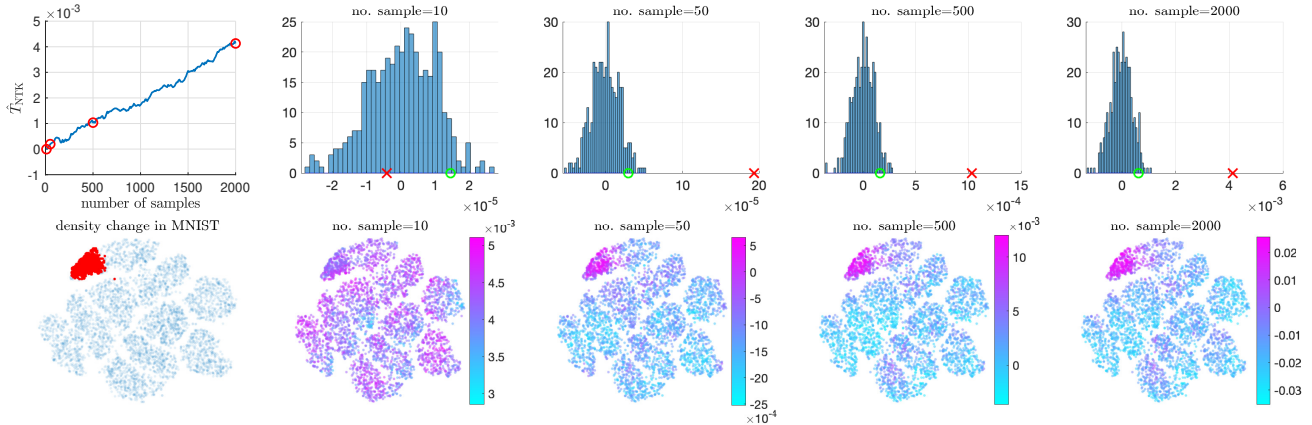


Figure 3: NTK-MMD statistic to detect distribution abundance change in MNIST digit image data; $n_{tr} = 2000$ and n_{te} is about 4000. (Top) Most left: Change of the statistic over the number of samples in the online training (batch size =1) of a 2-layer convolutional network. From 2nd-5th columns: The MMD statistic \hat{T}_a compared with the empirical distribution under H_0 via test-only bootstrap, at four times along the online training (red circles on the left plot). (Bottom) Most left: The change of distribution of MNIST dataset embedded in 2D by tSNE [46]. From 2nd-5th columns: The witness function \hat{g} plotted as a color field over the samples, at the four times corresponding to the upper panel plots.

Results. To verify the $O(t)$ discrepancy as in Proposition 2.1, we first compute the numerical values of \hat{T}_{NTK} and $\hat{T}_{\text{net}}(t)$ for different values of t (which corresponds to different learning rate α as explained in Remark 2.2 and Appendix A.2) and the relative approximation error defined as $\text{err} = |\hat{T}_{\text{net}}(t) - \hat{T}_{\text{NTK}}| / |\hat{T}_{\text{NTK}}|$. The results are shown in Figure A.1. The fitted scaling of the error for softplus activation is about 0.96, which agrees with the theoretical $O(t)$ error. Switching to relu, the order is not close to 1 (instead 0.62) but $\hat{T}_{\text{net}}(t)$ still gives a good approximation of \hat{T}_{NTK} as the relative error achieves about 10^{-3} . The comparison of the testing power of network approximate NTK statistic and the exact NTK statistic tests are shown in Figure 2. In the high dimensional Gaussian covariance shift test ($d = 100$), the powers of the three tests are similar. When reducing dimension to $d = 2$, the full-bootstrap NTK tests show slightly different testing power than the other two. The network approximate NTK and NTK with test-only bootstrap always show almost the same testing power, consistent with the theory in Subsection 2.3. In the experiment on \mathbb{R}^2 data, the estimated threshold by full-bootstrap is smaller than by test-only bootstrap (right two plots), which explains the possibly better-testing power.

4.3 Comparison to neural network classification two-sample tests

Set-up. We experimentally compare NTK-MMD and state-of-the-art classification two-sample test (C2ST) baselines, which are neural network based tests. Following [36], we compare with C2ST-S, the classification accuracy test [37], and C2ST-L, the classification logit test [10]. Experimental details are given in Appendix C.4. The data distributions are:

- Example 1: Gaussian mixture, fixed dimension $d = 10$ and increasing n_{tr} , which is the same setting as Figure 3 (left 2 plots) in [36]. Numbers in Table 1 show testing power (in %).
- Example 2: Modified Gaussian mixture (from Example 1), the covariance shift is $I + 0.1E$ in both mixtures, where E is all-one matrix with zeros on the diagonal. Dimension $d = 10$, and number of training samples n_{tr} increases. The test power is shown in Table 2.

Results. On Example 1, NTK-MMD performs similar to SCF test in most cases, better than C2ST-S (SGD 1-epoch), and is worse than the other baselines. On Example 2, NTK-MMD outperforms C2ST

n_{tr}	2000	4000	6000	8000
ME*	~ 10.0	~ 30.0	~ 58.0	~ 75.0
SCF*	~ 5.0	~ 6.0	~ 10.0	~ 15.0
C2ST-S (Adam)	9.9 (61.6)	14.0 (95.8)	39.1 (100.0)	61.2 (100.0)
C2ST-L (Adam)	14.1 (87.8)	38.4 (100.0)	76.4 (100.0)	92.9 (100.0)
C2ST-S (SGD)	6.0 (13.9)	10.6 (50.0)	10.8 (94.4)	14.8 (99.6)
C2ST-L (SGD)	6.7 (22.2)	12.8 (81.6)	22.1 (100.0)	34.6 (100.0)
NTK-MMD	7.1	9.6	13.7	17.9

Table 1: Test power on Gaussian mixture data Example 1, dimension $d = 10$. (*recovered from Figure 3 in [36], \sim means about.) For C2ST’s, the number outside brackets is for epoch = 1, and in brackets for epoch = 10.

n_{tr}	500	1000	1500	2000
C2ST-S (Adam)	21.8 (28.1)	62.2 (53.8)	79.4 (74.0)	94.6 (85.2)
C2ST-L (Adam)	48.5 (49.4)	92.8 (82.6)	99.5 (96.3)	100.0 (98.8)
C2ST-S (SGD)	7.4 (28.3)	22.7 (79.7)	35.3 (92.4)	54.9 (96.8)
C2ST-L (SGD)	18.3 (52.2)	56.8 (97.6)	81.4 (99.9)	97.3 (100.0)
NTK-MMD	34.3	68.9	88.8	95.9

Table 2: Test power on Gaussian mixture data Example 2, dimension $d = 10$.

baselines in several cases, e.g., constantly better than C2ST-S (SGD and Adam, 1-epoch) and comparable to C2ST-L (SGD 1-epoch). Note that C2ST baselines can be sensitive to training hyperparameters, such as the choice of optimization algorithm (SGD or Adam) and number of epochs. As far as the authors are aware of, there is no theoretical training guarantee of C2ST tests. In contrast, NTK-MMD has theoretical training guarantees due to the provable approximation to a kernel MMD. The weakness of NTK-MMD, though, is that the NTK kernel may not be discriminative to distinguish certain distribution departures, like in Example 1. The expressiveness power of NTK-MMD may be theoretically analyzed, for example, in the infinite-width limit using the analytical formula, as the infinite-width NTK has been shown to be universal for data on hyperspheres [28]. Overall, the results suggest that the performances of the three neural network tests depend on the data distributions, which is anticipated for any hypothesis test. Further theoretical investigations are postponed here.

4.4 MNIST distribution abundance change

Dataset. We take the original MNIST dataset, which contains 28×28 gray-scale images, and construct two densities p and q by subsampling from the 70000 images in 10 classes, following [12]: p is uniformly subsampled from the MNIST dataset, $p = p_{\text{data}}$, and q has a change of abundance $q = 0.85p_{\text{data}} + 0.15p_{\text{cohort}}$, where p_{cohort} is the distribution of a subset of the class of digit “1” having about 1900 samples. The p_{cohort} is illustrated in the left bottom plot in Figure 3. The two samples X and Y have $n_X = 3000$, $n_Y = 2981$, and we randomly split X and Y make the training set $\mathcal{D}_{tr} = \{X_{(1)}, Y_{(1)}\}$, $n_{X,(1)} = n_{Y,(1)} = 1000$, and the rest is the test set \mathcal{D}_{te} .

Results. Using a 2-layer convolutional neural network, we compute the network MMD statistic $\hat{T}_{a,\text{net}}$ (17) and the test-only bootstrap (18). The online training uses batch size =1 and one epoch, and more experimental details are in Appendix C.5. The results are shown in Figure 3. The NTK-MMD statistic already shows testing power after being trained on 50 samples, and in the later stage of training, the NTK witness function $\hat{g}_{(1)}$ identifies the region of the abundance change.

4.5 Online human activity change-point detection

Set-up. We present an illustrative example using NTK-MMD test statistic to perform online change-point detection: detecting human activity transition. We consider a real-world dataset, the Microsoft

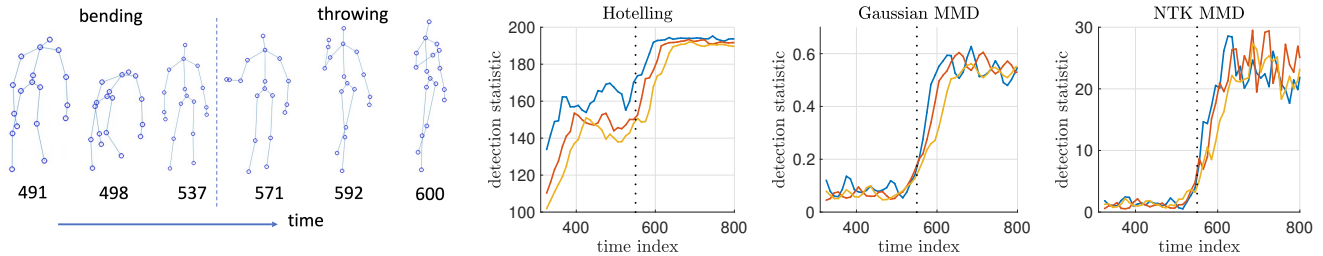


Figure 4: (Left) Example data sequence in the human activity dataset: before and after the change-point. (Right) Detection statistics computed by Hotelling’s T statistic, Gaussian MMD, and NTK MMD, on human action trajectory dataset, using window size 100 (blue), 150 (red), and 200 (yellow), respectively. The change point is at time index 550 (dotted black).

Research Cambridge-12 (MSRC-12) Kinect gesture dataset [18]. The data sequence records a human subject repetitively bending the body/picking up and throwing a ball before/after the change happens. After preprocessing, the sequential dataset contains 1192 frames (samples) and 54 attributes (data samples are in \mathbb{R}^{54}), with a change of action from “bending” to “throwing” at time index 550. More description of the dataset and experimental details is provided in Appendix C.6. Example samples before and after the change point are shown in the left of Figure 4. The algorithm is based on a sliding window which moves forward with time, and we compute the detection statistic every ten frames; such a procedure can be viewed as the Shewhart Chart in the literature [47]; scanning MMD statistic has been used in [32]. The window size is chosen to be 100, 150, and 200, respectively. We take a block of data (same size as the window) before the time index 300 (to use as the pilot samples) and compare with the distribution of data from the sliding window to compute the detection statistic. If there is a change-point, the detection statistic will show a large value.

Results. The other two detection statistics are computed by (i) Gaussian MMD (with bandwidth chosen to be median distance) and (ii) Hotelling’s T statistics. The results are shown in Figure 4, where both the Gaussian MMD and the NTK-MMD statistics can detect the change: the detection statistic value remains low before the change and remains high after the change point, and both are better than the Hotelling statistic.

5 Discussion

The current work can naturally be extended in several aspects. First, the analysis of NTK approximation error may be extended, e.g., to other activation functions, and under the infinite-width limit. Second, considering other training objectives may allow us to compare NTK-MMD to other neural network classification tests. At the same time, the limitation of lazy-regime training has been studied in [21, 22, 39], which indicates that NTK theory cannot fully characterize the modeling ability of deep networks. It has also been shown that the expressiveness of the NTK kernel may be restricted to certain limited type of kernels [8, 20, 9]. This motivates extensions of NTK for studying deep network training [26, 41]. Finally, the application may extend to various hypothesis testing tasks as well as deep generative models. We thus view the current work as a first step towards understanding the role and potential of trained neural networks in testing problems and applications.

Acknowledgement

The authors thank Alexander Cloninger and Galen Reeves for helpful discussion on the initial version of the paper, and the anonymous reviewers for helpful feedback. The work is supported by NSF DMS-

2134037. XC is partially supported by NSF, NIH and the Alfred P. Sloan Foundation. YX is partially supported by NSF (CAREER Award 1650913, DMS-1938106, and DMS-1830210).

References

- [1] Zeyuan Allen-Zhu, Yuanzhi Li, and Zhao Song. A convergence theory for deep learning via overparameterization. In *International Conference on Machine Learning*, pages 242–252. PMLR, 2019.
- [2] Niall H Anderson, Peter Hall, and D Michael Titterton. Two-sample test statistics for measuring discrepancies between two multivariate probability density functions using kernel-based density estimates. *Journal of Multivariate Analysis*, 50(1):41–54, 1994.
- [3] Michael Arbel, Anna Korba, Adil Salim, and Arthur Gretton. Maximum mean discrepancy gradient flow. *arXiv preprint arXiv:1906.04370*, 2019.
- [4] Miguel A Arcones and Evarist Gine. On the bootstrap of u and v statistics. *The Annals of Statistics*, pages 655–674, 1992.
- [5] Sanjeev Arora, Simon Du, Wei Hu, Zhiyuan Li, and Ruosong Wang. Fine-grained analysis of optimization and generalization for overparameterized two-layer neural networks. In *International Conference on Machine Learning*, pages 322–332. PMLR, 2019.
- [6] Sanjeev Arora, Simon S Du, Wei Hu, Zhiyuan Li, Russ R Salakhutdinov, and Ruosong Wang. On exact computation with an infinitely wide neural net. In *Advances in Neural Information Processing Systems*, pages 8139–8148, 2019.
- [7] Yuval Belfer, Amnon Geifman, Meirav Galun, and Ronen Basri. Spectral analysis of the neural tangent kernel for deep residual networks. *arXiv preprint arXiv:2104.03093*, 2021.
- [8] Alberto Bietti and Julien Mairal. On the inductive bias of neural tangent kernels. *arXiv preprint arXiv:1905.12173*, 2019.
- [9] Lin Chen and Sheng Xu. Deep neural tangent kernel and laplace kernel have the same rkhs. *arXiv preprint arXiv:2009.10683*, 2020.
- [10] Xiuyuan Cheng and Alexander Cloninger. Classification logit two-sample testing by neural networks. *arXiv preprint arXiv:1909.11298*, 2019.
- [11] Xiuyuan Cheng, Alexander Cloninger, and Ronald R Coifman. Two-sample statistics based on anisotropic kernels. *Information and Inference: A Journal of the IMA*, 9(3):677–719, 2020.
- [12] Xiuyuan Cheng and Yao Xie. Kernel two-sample tests for manifold data. *arXiv preprint arXiv:2105.03425*, 2021.
- [13] Lénaïc Chizat, Edouard Oyallon, and Francis Bach. On lazy training in differentiable programming. *Advances in Neural Information Processing Systems*, 32:2937–2947, 2019.
- [14] Kacper P Chwialkowski, Aaditya Ramdas, Dino Sejdinovic, and Arthur Gretton. Fast two-sample testing with analytic representations of probability measures. In *Advances in Neural Information Processing Systems*, pages 1981–1989, 2015.
- [15] Simon Du, Jason Lee, Haochuan Li, Liwei Wang, and Xiyu Zhai. Gradient descent finds global minima of deep neural networks. In *International Conference on Machine Learning*, pages 1675–1685. PMLR, 2019.

- [16] Simon S Du, Kangcheng Hou, Barnabás Póczos, Ruslan Salakhutdinov, Ruosong Wang, and Keyulu Xu. Graph neural tangent kernel: Fusing graph neural networks with graph kernels. *arXiv preprint arXiv:1905.13192*, 2019.
- [17] Simon S Du, Xiyu Zhai, Barnabas Poczos, and Aarti Singh. Gradient descent provably optimizes over-parameterized neural networks. In *International Conference on Learning Representations*, 2018.
- [18] Simon Fothergill, Helena Mentis, Pushmeet Kohli, and Sebastian Nowozin. Instructing people for training gestural interactive systems. In *Proceedings of the SIGCHI Conference on Human Factors in Computing Systems*, pages 1737–1746, 2012.
- [19] Jerome Friedman. On multivariate goodness-of-fit and two-sample testing. Technical report, Stanford Linear Accelerator Center, Menlo Park, CA (US), 2004.
- [20] Amnon Geifman, Abhay Yadav, Yoni Kasten, Meirav Galun, David Jacobs, and Ronen Basri. On the similarity between the laplace and neural tangent kernels. *arXiv preprint arXiv:2007.01580*, 2020.
- [21] Behrooz Ghorbani, Song Mei, Theodor Misiakiewicz, and Andrea Montanari. Limitations of lazy training of two-layers neural networks. *arXiv preprint arXiv:1906.08899*, 2019.
- [22] Behrooz Ghorbani, Song Mei, Theodor Misiakiewicz, and Andrea Montanari. When do neural networks outperform kernel methods? *arXiv preprint arXiv:2006.13409*, 2020.
- [23] Arthur Gretton, Karsten M Borgwardt, Malte J Rasch, Bernhard Schölkopf, and Alexander Smola. A kernel two-sample test. *Journal of Machine Learning Research*, 13(Mar):723–773, 2012.
- [24] Arthur Gretton, Philipp Hennig, Carl Edward Rasmussen, and Bernhard Schölkopf. New directions for learning with kernels and gaussian processes (dagstuhl seminar 16481). In *Dagstuhl Reports*, volume 6. Schloss Dagstuhl-Leibniz-Zentrum fuer Informatik, 2017.
- [25] Arthur Gretton, Dino Sejdinovic, Heiko Strathmann, Sivaraman Balakrishnan, Massimiliano Pontil, Kenji Fukumizu, and Bharath K Sriperumbudur. Optimal kernel choice for large-scale two-sample tests. In *Advances in neural information processing systems*, pages 1205–1213, 2012.
- [26] Jiaoyang Huang and Horng-Tzer Yau. Dynamics of deep neural networks and neural tangent hierarchy. In *International Conference on Machine Learning*, pages 4542–4551. PMLR, 2020.
- [27] Kaixuan Huang, Yuqing Wang, Molei Tao, and Tuo Zhao. Why do deep residual networks generalize better than deep feedforward networks?—a neural tangent kernel perspective. *Advances in Neural Information Processing Systems*, 33, 2020.
- [28] Arthur Jacot, Franck Gabriel, and Clément Hongler. Neural tangent kernel: convergence and generalization in neural networks. In *Proceedings of the 32nd International Conference on Neural Information Processing Systems*, pages 8580–8589, 2018.
- [29] Wittawat Jitkrittum, Zoltán Szabó, Kacper P Chwialkowski, and Arthur Gretton. Interpretable distribution features with maximum testing power. In *Advances in Neural Information Processing Systems*, pages 181–189, 2016.
- [30] Jonas M Kübler, Wittawat Jitkrittum, Bernhard Schölkopf, and Krikamol Muandet. Learning kernel tests without data splitting. *Advances in Neural Information Processing Systems*, 2020.
- [31] Chun-Liang Li, Wei-Cheng Chang, Yu Cheng, Yiming Yang, and Barnabás Póczos. Mmd gan: Towards deeper understanding of moment matching network. In *Advances in Neural Information Processing Systems*, pages 2203–2213, 2017.

- [32] Shuang Li, Yao Xie, Hanjun Dai, and Le Song. Scan b-statistic for kernel change-point detection. *Sequential Analysis*, 38(4):503–544, 2019.
- [33] Yuanzhi Li and Yingyu Liang. Learning overparameterized neural networks via stochastic gradient descent on structured data. In *Proceedings of the 32nd International Conference on Neural Information Processing Systems*, pages 8168–8177, 2018.
- [34] Yujia Li, Kevin Swersky, and Rich Zemel. Generative moment matching networks. In *International Conference on Machine Learning*, pages 1718–1727, 2015.
- [35] Zhiyuan Li, Ruosong Wang, Dingli Yu, Simon S Du, Wei Hu, Ruslan Salakhutdinov, and Sanjeev Arora. Enhanced convolutional neural tangent kernels. *arXiv preprint arXiv:1911.00809*, 2019.
- [36] Feng Liu, Wenkai Xu, Jie Lu, Guangquan Zhang, Arthur Gretton, and DJ Sutherland. Learning deep kernels for non-parametric two-sample tests. *arXiv preprint arXiv:2002.09116*, 2020.
- [37] David Lopez-Paz and Maxime Oquab. Revisiting classifier two-sample tests. In *International Conference on Learning Representations*, 2017.
- [38] Aaditya Ramdas, Sashank Jakkam Reddi, Barnabás Póczos, Aarti Singh, and Larry Wasserman. On the decreasing power of kernel and distance based nonparametric hypothesis tests in high dimensions. In *Twenty-Ninth AAAI Conference on Artificial Intelligence*, 2015.
- [39] Maria Refinetti, Sebastian Goldt, Florent Krzakala, and Lenka Zdeborová. Classifying high-dimensional gaussian mixtures: Where kernel methods fail and neural networks succeed. *arXiv preprint arXiv:2102.11742*, 2021.
- [40] Mark D Reid and Robert C Williamson. Information, divergence and risk for binary experiments. *Journal of Machine Learning Research*, 12(Mar):731–817, 2011.
- [41] Daniel A Roberts, Sho Yaida, and Boris Hanin. The principles of deep learning theory. *arXiv preprint arXiv:2106.10165*, 2021.
- [42] Robert J Serfling. *Approximation theorems of mathematical statistics*, 1981.
- [43] Bharath K Sriperumbudur, Kenji Fukumizu, Arthur Gretton, Bernhard Schölkopf, and Gert RG Lanckriet. On integral probability metrics, ϕ -divergences and binary classification. *arXiv preprint arXiv:0901.2698*, 2009.
- [44] Dougal J Sutherland, Hsiao-Yu Tung, Heiko Strathmann, Soumyajit De, Aaditya Ramdas, Alex Smola, and Arthur Gretton. Generative models and model criticism via optimized maximum mean discrepancy. *arXiv preprint arXiv:1611.04488*, 2016.
- [45] Tom Tirer, Joan Bruna, and Raja Giryes. Kernel-based smoothness analysis of residual networks. *arXiv preprint arXiv:2009.10008*, 2020.
- [46] Laurens Van Der Maaten. Accelerating t-sne using tree-based algorithms. *The Journal of Machine Learning Research*, 15(1):3221–3245, 2014.
- [47] Liyan Xie, Shaofeng Zou, Yao Xie, and Venugopal V Veeravalli. Sequential (quickest) change detection: Classical results and new directions. *IEEE Journal on Selected Areas in Information Theory*, 2021.
- [48] Difan Zou, Yuan Cao, Dongruo Zhou, and Quanquan Gu. Gradient descent optimizes overparameterized deep relu networks. *Machine Learning*, 109(3):467–492, 2020.

A Proofs and additional analysis in Section 2

A.1 Proofs in Section 2.3

Remark A.1 (Biased and unbiased MMD estimators). The exact NTK-MMD statistic (9) is a biased estimator [23]. The unbiased estimator is by excluding the diagonal terms of kernel matrix in the summation and normalizing by “ $1/n(n-1)$ ” instead of “ $1/n^2$ ”. We consider biased estimator for simplicity, and also because the testing power analysis gives similar results, c.f. the comment beneath Theorem 3.1. In addition, the “asymmetric MMD statistic” (16) (with training-test splitting and used in many practical situations) is an unbiased estimator.

Proof of Lemma 2.1. By (3),

$$\frac{\partial \hat{L}}{\partial \theta} = - \int_{\mathcal{X}} \nabla_{\theta} f(x; \theta) (\hat{p} - \hat{q})(x) dx. \quad (22)$$

By the GD training dynamic,

$$\frac{\partial}{\partial t} u(x, t) = \langle \nabla_{\theta} f(x, \theta(t)), \dot{\theta}(t) \rangle \quad (23)$$

$$= \left\langle \nabla_{\theta} f(x, \theta(t)), -\frac{\partial \hat{L}}{\partial \theta} \right\rangle \quad (24)$$

$$= \int_{\mathcal{X}} \langle \nabla_{\theta} f(x; \theta(t)), \nabla_{\theta} f(x'; \theta(t)) \rangle (\hat{p} - \hat{q})(x') dx'. \quad (25)$$

This proves the lemma by definition of $\hat{K}_t(x, x')$ in (6). \square

Proof of Lemma 2.2. To prove Part (1): The initial weights $\theta(0) \in \Theta$, and by Taylor expansion,

$$\theta(t) = \theta(0) + t\dot{\theta}(t'),$$

from $0 < t' < t < t_{f,r}$. By definition,

$$\dot{\theta}(t') = - \frac{\partial \hat{L}}{\partial \theta} \Big|_{\theta=\theta(t')} = \int_{\mathcal{X}} \nabla_{\theta} f(x; \theta(t')) (\hat{p} - \hat{q})(x) dx, \quad (26)$$

and thus by that $\|\nabla_{\theta} f\|_{\mathcal{X}, \Theta} \leq L_f$.

$$\|\dot{\theta}(t')\| \leq 2L_f,$$

This give that $\|\theta(t) - \theta(0)\| \leq t2L_f$, which proves Part (1).

To prove Part (2): Note that for any x, x' , and $t < t_{f,r}$,

$$\frac{\partial}{\partial t} \hat{K}_t(x, x') = R_t(x, x') + R_t(x', x), \quad R_t(x, x') := \langle D_{\theta}^2 f(x, \theta(t)) (\dot{\theta}(t)), \nabla_{\theta} f(x', \theta(t)) \rangle.$$

By Taylor expansion, for some $0 < t' < t$,

$$\hat{K}_t(x, x') = K_0(x, x') + t(R_{t'}(x, x') + R_{t'}(x', x))$$

where by part (1), $\theta(t') \in B_r$. Again by (26), this gives that

$$\|\dot{\theta}(t')\| \leq 2\|\nabla_{\theta} f\|_{\mathcal{X}, B_r},$$

where note that the domain of θ is $B_r \subset \Theta$, and thus the constant $\|\nabla_{\theta} f\|_{\mathcal{X}, B_r}$ can potentially be smaller than L_f . Then,

$$\|D_{\theta}^2 f(x, \theta(t'))(\dot{\theta}(t'))\| \leq 2\|D_{\theta}^2 f\|_{\mathcal{X}, B_r} \|\nabla_{\theta} f\|_{\mathcal{X}, B_r}.$$

As a result,

$$|R_{t'}(x, x')| \leq \|D_{\theta}^2 f(x, \theta(t'))(\dot{\theta}(t'))\| \|\nabla_{\theta} f(x', \theta(t'))\| \leq 2\|D_{\theta}^2 f\|_{\mathcal{X}, B_r} \|\nabla_{\theta} f\|_{\mathcal{X}, B_r}^2.$$

The same bound holds for $|R_{t'}(x, x')|$, and the above bounds are uniformly for all x, x' . Putting together, this proves Part (2). \square

Proof of Proposition 2.1. By definition,

$$\begin{aligned} \hat{T}_{net}(t) - \hat{T}_{\text{NTK}} &= \int_{\mathcal{X}} \int_{\mathcal{X}} \frac{1}{t} \int_0^t \left(\hat{K}_s(x, x') - K_0(x, x') \right) ds (\hat{p} - \hat{q})(x') dx' (\hat{p} - \hat{q})(x) dx \\ &= \int_{\mathcal{X}} \int_{\mathcal{X}} E(x, x') \hat{p}(x') \hat{p}(x) dx' dx - \int_{\mathcal{X}} \int_{\mathcal{X}} E(x, x') \hat{p}(x') \hat{q}(x) dx' dx \\ &\quad - \int_{\mathcal{X}} \int_{\mathcal{X}} E(x, x') \hat{q}(x') \hat{p}(x) dx' dx + \int_{\mathcal{X}} \int_{\mathcal{X}} E(x, x') \hat{q}(x') \hat{q}(x) dx' dx \end{aligned} \quad (27)$$

where we define

$$E(x, x') := \frac{1}{t} \int_0^t \left(\hat{K}_s(x, x') - K_0(x, x') \right) ds.$$

By Lemma 2.2, for $t < t_{f,r}$ and for any $x, x' \in \mathcal{X}$

$$|E(x, x')| \leq \frac{1}{t} \int_0^t \left| \hat{K}_s(x, x') - K_0(x, x') \right| ds \leq \frac{1}{t} \int_0^t C_{f,r} s ds = \frac{t}{2} C_{f,r}.$$

Thus the four terms in (27) in absolute value are all upper bounded by $C_{f,r}t/2$, and thus $|\hat{T}_{net}(t) - \hat{T}_{\text{NTK}}|$ is upper bounded by the sum of the absolute values of the four terms which is less than or equal to $2C_{f,r}t$. \square

A.2 Extension to SGD training

Consider the online setting of training the network by minimizing the loss $\hat{L}(\theta)$ in (3) on $n = n_X + n_Y$ samples. We write the training set $\mathcal{D}_{tr} = \{(z_i, l_i)\}_{i=1}^n$, where z_i is from X or Y , and $l_i = 1$ or 2 is the class label. Let $b_i = 1/n_X$ if $l_i = 1$, and $1/n_Y$ if $l_i = 2$. The loss can be written as

$$\hat{L}(\theta) = \sum_{i=1}^n f(z_i; \theta) b_i, \quad b_i = \begin{cases} -1/n_X, & l_i = 1, \\ 1/n_Y, & l_i = 2. \end{cases}$$

For simplicity, assume that $n_X = n_Y = n/2$. We define $l_i(\theta) = b_i f(z_i; \theta)$, which is the loss from the i -th sample.

Suppose we train the network with batch size =1 and 1 epoch. The learning rate is α , that is, for k -th iteration in the SGD, $k = 1, \dots, n$,

$$\theta_k = \theta_{k-1} - \alpha \nabla_{\theta} l_k(\theta_{k-1}),$$

from some $\theta_0 \in \Theta$. Note that $\nabla_{\theta} l_k(\theta) = b_k \nabla_{\theta} f(z_k; \theta)$, and thus

$$\|\theta_k - \theta_{k-1}\| = \alpha \|\nabla_{\theta} l_k(\theta_{k-1})\| = \alpha |b_k| \|\nabla_{\theta} f(z_k; \theta_{k-1})\| \leq 2L_f \frac{\alpha}{n}. \quad (28)$$

This implies that

$$\|\theta_k - \theta_0\| \leq 2L_f \frac{k}{n} \alpha, \quad (29)$$

and in particular, $\|\theta_n - \theta_0\| \leq 2L_f \alpha$. Thus, θ_k for all k up to n stays in a r -Euclidean ball of θ_0 if $2L_f \alpha < r$.

We write the network function at k -th step as u_k , $u_k(x) = f(x; \theta_k)$.

$$\begin{aligned} u_k(x) - u_{k-1}(x) &= f(x; \theta_k) - f(x; \theta_{k-1}) \\ &= \nabla_{\theta} f(x; \theta_{k-1})^T (\theta_k - \theta_{k-1}) + O(\|\theta_k - \theta_{k-1}\|^2) \\ &= -\alpha b_k \nabla_{\theta} f(x; \theta_{k-1})^T \nabla_{\theta} f(z_k; \theta_{k-1}) + O\left(\left(\frac{\alpha}{n}\right)^2\right), \end{aligned} \quad (30)$$

where we treat L_f as $O(1)$ constant, and the same with other constants which depend on the infinity norm of derivatives of f .

We analyze how $\nabla_{\theta} f(x; \theta_{k-1})^T \nabla_{\theta} f(z_k; \theta_{k-1})$ differs from $\nabla_{\theta} f(x; \theta_0)^T \nabla_{\theta} f(z_k; \theta_0)$. For any $x \in \mathcal{X}$,

$$\nabla_{\theta} f(x; \theta_{k-1}) = \nabla_{\theta} f(x; \theta_0) + O(\|\theta_{k-1} - \theta_0\|),$$

and by (29),

$$\nabla_{\theta} f(x; \theta_{k-1}) = \nabla_{\theta} f(x; \theta_0) + O\left(\frac{k-1}{n} \alpha\right).$$

Thus,

$$\begin{aligned} \nabla_{\theta} f(x; \theta_{k-1})^T \nabla_{\theta} f(z_k; \theta_{k-1}) &= \left\langle \nabla_{\theta} f(x; \theta_0) + O\left(\frac{k-1}{n} \alpha\right), \nabla_{\theta} f(z_k; \theta_0) + O\left(\frac{k-1}{n} \alpha\right) \right\rangle \\ &= \nabla_{\theta} f(x; \theta_0)^T \nabla_{\theta} f(z_k; \theta_0) + O\left(\frac{k-1}{n} \alpha\right). \end{aligned}$$

Back to (30), we have

$$\begin{aligned} u_k(x) - u_{k-1}(x) &= -\alpha b_k \left(\nabla_{\theta} f(x; \theta_0)^T \nabla_{\theta} f(z_k; \theta_0) + O\left(\frac{k-1}{n} \alpha\right) \right) + O\left(\left(\frac{\alpha}{n}\right)^2\right) \\ &= -\alpha b_k \nabla_{\theta} f(x; \theta_0)^T \nabla_{\theta} f(z_k; \theta_0) + O\left(\frac{k-1}{n^2} \alpha^2\right) + O\left(\left(\frac{\alpha}{n}\right)^2\right). \end{aligned}$$

This give that

$$\begin{aligned} u_n(x) - u_0(x) &= -\alpha \sum_{k=1}^n b_k \nabla_{\theta} f(x; \theta_0)^T \nabla_{\theta} f(z_k; \theta_0) + \sum_{k=1}^n O\left(k \frac{\alpha^2}{n^2}\right) \\ &= \alpha \int_{\mathcal{X}} K_0(x, x') (\hat{p} - \hat{q})(x') dx' + O(\alpha^2), \end{aligned}$$

where recall that $K_0(x, x') = \nabla_{\theta} f(x; \theta_0)^T \nabla_{\theta} f(x'; \theta_0)$ is the NTK at time zero. This proves that

$$\hat{g}(x) := \frac{1}{\alpha} (u_n(x) - u_0(x)) = \int_{\mathcal{X}} K_0(x, x') (\hat{p} - \hat{q})(x') dx' + O(\alpha).$$

Comparing to the continuous time training dynamic, we see that α corresponds to training time t , and with batch size 1 the SGD training the NTK approximation has the same $O(\alpha)$ error as with the continuous time GD training.

B Proofs and additional theoretical results in Section 3

B.1 Proofs in Subsection 3.1

The proof of Theorem 3.1 uses the U-statistic concentration analysis, which was used in Theorem 3.5 in [12]. The analysis in [12] is for the local RBF kernel, and we need to extend to the general PSD kernel here.

The concentration argument is by Proposition B.1. Note that the concentration can be derived using the boundedness (11) alone, while the Bernstein-type control here is sharper when the squared integrals upper bound ν is much smaller than 1.

Proposition B.1 (Concentration of \hat{T}_{NTK}). *Assuming (11), (14) and the conditions (i) and (ii) in Theorem 3.1,*

- (1) Under H_0 , when $0 < \lambda < 3\sqrt{c\nu n}$, w.p. $\geq 1 - 3e^{-\lambda^2/8}$, $\hat{T} \leq \frac{4}{cn} + 4\lambda\sqrt{\frac{\nu}{cn}}$.
- (2) Under H_1 , when $0 < \lambda < 3\sqrt{c\nu n}$, w.p. $\geq 1 - 3e^{-\lambda^2/8}$, $\hat{T} \geq \delta_K - 4\lambda\sqrt{\frac{\nu}{cn}}$.

The proof of Theorem 3.1 is a direct application of the proposition.

Proof of Theorem 3.1. Note that condition (15) ensures that

$$\max\{\lambda_1, \lambda_2\} < 3\sqrt{c\nu n}, \quad \frac{4}{cn} < 0.5\delta_K, \quad 4(\lambda_1 + \lambda_2)\sqrt{\frac{\nu}{cn}} < 0.5\delta_K, \quad (31)$$

and the bounds in Proposition B.1 parts (1) and (2) hold with λ_1 and λ_2 respectively.

To verify that $\mathbb{P}[\hat{T} > t_{\text{thres}}] \leq \alpha_{\text{level}}$ under H_0 : Observe that $3e^{-\lambda_1^2/8} = \alpha_{\text{level}}$ by the definition of λ_1 , and then the claim follows by Proposition B.1 Part (1) since $\lambda_1 < 3\sqrt{c\nu n}$.

To bound $\mathbb{P}[\hat{T} \leq t_{\text{thres}}]$ under H_1 : Since $\lambda_2 < 3\sqrt{c\nu n}$, by Proposition B.1 Part (1), the claim holds if

$$t_{\text{thres}} = \frac{4}{cn} + 4\lambda_1\sqrt{\frac{\nu}{cn}} < \delta_K - 4\lambda_2\sqrt{\frac{\nu}{cn}}, \quad (32)$$

which is guaranteed by (31). □

Remark B.1 (Asymptotic choice of t_{thres}). The optimal t_{thres} in Theorem 3.1 as the $(1 - \alpha_{\text{level}})$ -quantile of the distribution of \hat{T} under H_0 can be obtained potentially analytically according to the limiting distribution of the MMD statistic: The asymptotic distribution of (squared) empirical MMD statistic has been derived using the spectral decomposition of the (centered) kernel function $\tilde{k}(x, x') := K(x, x') - \mathbb{E}_{y \sim p} K(x, y) - \mathbb{E}_{y \sim p} K(y, x') + \mathbb{E}_{y, y' \sim p} K(y, y')$ in [23, 11], among others, following techniques in Chapter 6 in [42]. Specifically, by Theorem 3.3 in [11], as $n = n_X + n_Y \rightarrow \infty$ and $n_X/n \rightarrow \rho_X \in (0, 1)$, $n\hat{T}$ under H_0 , $q = p$, converges in distribution to the weighted χ^2 distribution $\sum_{k=1}^{\infty} \tilde{\lambda}_k \xi_k^2$, where $\xi_k \sim \mathcal{N}(0, 1/\rho_X + 1/(1 - \rho_X))$ i.i.d, and $\tilde{\lambda}_k \geq 0$ are the eigenvalues of the integral operator with kernel $\tilde{k}(x, x')$ in $L^2(\mathcal{X}, p(x)dx)$. This provides the asymptotic value of the quantile of \hat{T} under H_0 , when the eigenvalues are computable, which can be useful, e.g., for low-dimensional data.

Proof of Proposition B.1. The proof follows the approach in Proposition. 3.4 in [12]. By definition,

$$\hat{T} := \frac{1}{n_X^2} \sum_{i,j=1}^{n_X} K(x_i, x_j) + \frac{1}{n_Y^2} \sum_{i,j=1}^{n_Y} K(y_i, y_j) - \frac{2}{n_X n_Y} \sum_{i=1}^{n_X} \sum_{j=1}^{n_Y} K(x_i, y_j), \quad (33)$$

and equivalently,

$$\hat{T} = \hat{T}_{X,X} + \hat{T}_{Y,Y} - 2\hat{T}_{X,Y}, \quad (34)$$

$$\hat{T}_{X,X} = \frac{1}{n_X^2} \sum_{i,j=1}^{n_X} K(x_i, x_j), \quad \hat{T}_{Y,Y} = \frac{1}{n_Y^2} \sum_{i,j=1}^{n_Y} K(y_i, y_j), \quad \hat{T}_{X,Y} = \frac{1}{n_X n_Y} \sum_{i=1}^{n_X} \sum_{j=1}^{n_Y} K(x_i, y_j). \quad (35)$$

The terms $\hat{T}_{X,X}$ and $\hat{T}_{Y,Y}$ contain diagonal entries of the kernel matrix which have different marginal distributions from the off-diagonal entries. Define

$$D_X := \frac{1}{n_X} \sum_{i=1}^{n_X} K(x_i, x_i), \quad V_{X,X} := \frac{1}{n_X(n_X - 1)} \sum_{i \neq j, i,j=1}^{n_X} K(x_i, x_j),$$

then

$$\hat{T}_{X,X} = \frac{1}{n_X} D_X + \left(1 - \frac{1}{n_X}\right) V_{X,X} = V_{X,X} + \frac{1}{n_X} (D_X - V_{X,X}). \quad (36)$$

Observe that

$$\begin{aligned} |V_{X,X}| &\leq \frac{1}{n_X(n_X - 1)} \sum_{i \neq j, i,j=1}^{n_X} |K(x_i, x_j)| \\ &\leq \frac{1}{n_X(n_X - 1)} \sum_{i \neq j, i,j=1}^{n_X} \sqrt{K(x_i, x_i)} \sqrt{K(x_j, x_j)} \quad (K(x, x') \text{ is PSD}) \\ &\leq \frac{1}{n_X(n_X - 1)} \sum_{i \neq j, i,j=1}^{n_X} \frac{1}{2} (K(x_i, x_i) + K(x_j, x_j)) \\ &= \frac{1}{n_X} \sum_{i=1}^{n_X} K(x_i, x_i) = D_X, \end{aligned}$$

and, in addition, by (11),

$$0 \leq D_X \leq 1.$$

Thus (36) gives that

$$V_{X,X} \leq \hat{T}_{X,X} \leq V_{X,X} + \frac{2}{n_X} D_X \leq V_{X,X} + \frac{2}{n_X}. \quad (37)$$

The random variable $V_{X,X}$ is a U-statistic, where for $i \neq j$,

$$\mathbb{E}K(x_i, x_j) = \mathbb{E}_{x \sim p, y \sim p} K(x, y),$$

and by condition (ii),

$$\text{Var}(K(x_i, x_j)) \leq \mathbb{E}_{x \sim p, y \sim p} K(x, y)^2 = \nu_{p,p} \leq \nu.$$

As for the boundedness of the r.v. $K(x_i, x_j)$, by (11),

$$|K(x_i, x_j)| \leq 1 = L.$$

By the de-coupling of U-statistic in Proposition. 3.4 in [12], we obtain the Bernstein-type control of the tail probability, that is

$$\mathbb{P}[V_{X,X} - \mathbb{E}_{x \sim p, y \sim p} K(x, y) > t] \leq \exp\left\{-\frac{\frac{n_X-1}{2} t^2}{2\nu + \frac{2}{3} tL}\right\}, \quad \forall t > 0.$$

Let $t = \lambda\sqrt{\frac{\nu}{n_X-1}}$, to obtain the sub-Gaussian tail we need $tL < 3\nu$, that is, $t < 3\nu$ by that $L = 1$. This gives that when $0 < \lambda < 3\sqrt{\nu(n_X - 1)}$,

$$\mathbb{P}\left[V_{X,X} - \mathbb{E}_{x\sim p, y\sim p}K(x, y) > \lambda\sqrt{\frac{\nu}{n_X - 1}}\right] \leq \exp\left\{-\frac{(n_X - 1)t^2}{8\nu}\right\} = e^{-\lambda^2/8}.$$

The same holds for $\mathbb{P}\left[V_{X,X} - \mathbb{E}_{x\sim p, y\sim p}K(x, y) < -\lambda\sqrt{\frac{\nu}{n_X-1}}\right]$. Meanwhile, by (14),

$$cn \leq n_X - 1.$$

Together with (37), this gives that when $0 < \lambda < 3\sqrt{\nu cn}$,

$$\begin{aligned}\hat{T}_{X,X} &\leq \mathbb{E}_{x\sim p, y\sim p}K(x, y) + \lambda\sqrt{\frac{\nu}{cn}} + \frac{2}{cn}, \quad \text{w.p.} \geq 1 - e^{-\lambda^2/8}, \\ \hat{T}_{X,X} &\geq \mathbb{E}_{x\sim p, y\sim p}K(x, y) - \lambda\sqrt{\frac{\nu}{cn}}, \quad \text{w.p.} \geq 1 - e^{-\lambda^2/8}.\end{aligned}\tag{38}$$

The similar bound can be proved for $\hat{T}_{Y,Y}$, by defining D_Y and $V_{Y,Y}$ similarly, and using that $\nu_{q,q} \leq \nu$ and $cn \leq n_Y - 1$.

To analyze the concentration of $\hat{T}_{X,Y}$, which consists of the summation over the n_X -by- n_Y array, the de-coupling argument gives that for $M := \min\{n_X, n_Y\}$, and any $0 < \lambda < 3\sqrt{\nu M}$,

$$\mathbb{P}\left[\hat{T}_{X,Y} > \mathbb{E}_{x\sim p, y\sim q}K(x, y) + \lambda\sqrt{\frac{\nu}{M}}\right] \leq e^{-\lambda^2/8},$$

and same for $\mathbb{P}\left[\hat{T}_{X,Y} < \mathbb{E}_{x\sim p, y\sim q}K(x, y) - \lambda\sqrt{\frac{\nu}{M}}\right]$. By that $cn \leq M$, when $0 < \lambda < 3\sqrt{\nu cn}$,

$$\begin{aligned}\hat{T}_{X,Y} &\leq \mathbb{E}_{x\sim p, y\sim q}K(x, y) + \lambda\sqrt{\frac{\nu}{cn}}, \quad \text{w.p.} \geq 1 - e^{-\lambda^2/8}, \\ \hat{T}_{X,Y} &\geq \mathbb{E}_{x\sim p, y\sim q}K(x, y) - \lambda\sqrt{\frac{\nu}{cn}}, \quad \text{w.p.} \geq 1 - e^{-\lambda^2/8}.\end{aligned}\tag{39}$$

Finally, to prove Part (1) of the proposition, use the upper bound in (38), the corresponding upper bound for $\hat{T}_{Y,Y}$, and the lower bound in (39). This gives that, when $0 < \lambda < 3\sqrt{\nu cn}$, under the intersection of the three good events, which happens w.p. $\geq 1 - 3e^{-\lambda^2/8}$, we have that

$$\hat{T}_{X,X} + \hat{T}_{Y,Y} - 2\hat{T}_{X,Y} \leq (\mathbb{E}_{x\sim p, y\sim p} + \mathbb{E}_{x\sim q, y\sim q} - 2\mathbb{E}_{x\sim p, y\sim q})K(x, y) + 4\lambda\sqrt{\frac{\nu}{cn}} + \frac{4}{cn},$$

where the first term vanishes since $p = q$ under H_0 . To prove part (2), use the lower bounds in (38), in the counterpart of (38) for $\hat{T}_{Y,Y}$, and the upper bound in (39). \square

B.2 Proof of Theorem 3.2

In the proof of Theorem 3.2 and 3.3 which involves training and testing splitting, we use subscript (1) to denote the randomness over \mathcal{D}_{tr} , and subscript (2) that over \mathcal{D}_{te} , possibly conditioned on \mathcal{D}_{tr} . We use the notations $\mathbb{P}_{(i)}$, $\mathbb{E}_{(i)}$ and $\text{Var}_{(i)}$, for $i = 1, 2$. We say E is a good event in $\mathbb{P}_{(1)}$ which happens w.p. $\geq 1 - \delta$ in $\mathbb{P}_{(1)}$ if $\mathbb{P}_{(1)}[E^c] \leq \delta$, where $0 < \delta < 1$ is a small number.

Theorem 3.2 is based on Lemma B.1 which establishes the concentration of the conditional expectation $\mathbb{E}[\hat{T}_a|\mathcal{D}_{tr}]$, and Proposition B.2 on the concentration of \hat{T}_a under good events of \mathcal{D}_{tr} .

Proof of Theorem 3.2. We first consider under H_0 , where $\delta_K = 0$. Let $\gamma = 8\delta$, and applying Lemma B.1 with $\lambda_{(1)}$ such that

$$e^{-\lambda_{(1)}^2/4} = \delta,$$

which gives the same value of $\lambda_{(1)}$ as in the statement of the theorem. We have that there is a good event E_1 in $\mathbb{P}_{(1)}$, which happens w.p. $\geq 1 - 4\delta$, such that under E_1 ,

$$\hat{C} \leq \delta_K + 4\lambda_{(1)}\sqrt{\frac{\nu}{c_a n}} = 4\lambda_{(1)}\sqrt{\frac{\nu}{c_a n}}, \quad (40)$$

and this requires

$$\lambda_{(1)} < 3\sqrt{\nu c_a n}. \quad (41)$$

Applying Proposition B.2 (1), there is another good event E_2 in $\mathbb{P}_{(1)}$, which happens w.p. $\geq 1 - 4\delta$, such that under E_2 ,

$$\mathbb{P}_{(2)} \left[\hat{T}_a > \hat{C} + 4\lambda_{(2),1}\sqrt{\frac{1.1\nu}{c_a n}} \right] \leq 4e^{-\lambda_{(2),1}^2/4}, \quad (42)$$

as long as

$$\lambda_{(2),1} < 3\sqrt{1.1\nu c_a n}, \quad \sqrt{\log(1/\delta)/(2c_a n)} = \sqrt{\lambda_{(1)}^2/(8c_a n)} \leq 0.1\nu. \quad (43)$$

We thus set

$$4e^{-\lambda_{(2),1}^2/4} = \alpha_{\text{level}}, \quad t_{\text{thres}} = 4\lambda_{(1)}\sqrt{\frac{\nu}{c_a n}} + 4\lambda_{(2),1}\sqrt{\frac{1.1\nu}{c_a n}},$$

which gives the same values of $\lambda_{(2),1}$ and t_{thres} as in the statement of the theorem. Then, under the intersection event $E_1 \cap E_2$ which happens w.p. $\geq 1 - 8\delta = 1 - \gamma$ in $\mathbb{P}_{(1)}$, combining (40) and (42) gives that

$$\mathbb{P}[\hat{T}_a > t_{\text{thres}}] \leq \alpha_{\text{level}}.$$

Next, under H_1 , similarly, there are good events E'_1 and E'_2 , the intersection of which happens w.p. $\geq 1 - \gamma$ in $\mathbb{P}_{(1)}$, and under $E'_1 \cap E'_2$,

$$\hat{C} \geq \delta_K - 4\lambda_{(1)}\sqrt{\frac{\nu}{c_a n}},$$

and

$$\mathbb{P}_{(2)} \left[\hat{T}_a < \hat{C} - 4\lambda_{(2),2}\sqrt{\frac{1.1\nu}{c_a n}} \right] \leq 4e^{-\lambda_{(2),2}^2/4},$$

and this requires

$$\lambda_{2,(2)} < 3\sqrt{1.1\nu c_a n}. \quad (44)$$

This means that the Type-II error bound under H_1 in the theorem holds as long as

$$\delta_K - 4\lambda_{(1)}\sqrt{\frac{\nu}{c_a n}} - 4\lambda_{2,(2)}\sqrt{\frac{1.1\nu}{c_a n}} > t_{\text{thres}}. \quad (45)$$

Collecting the needed requirements (41) (43) (44) (45), and they are satisfied by (20) and the assumption of the theorem. \square

In both Lemma B.1 and Proposition B.2, suppose that (11), (19) and the conditions (i) and (ii) in Theorem 3.1 hold. We define the witness function of exact NTK MMD as

$$\hat{g}_{\text{NTK}}(x) := \int_{\mathcal{X}} K(x, x')(\hat{p}_{(1)} - \hat{q}_{(1)})(x') dx'. \quad (46)$$

Lemma B.1. Denote the conditional expectation $\mathbb{E}[\hat{T}_a | \mathcal{D}_{tr}]$ as

$$\hat{C} := \int_{\mathcal{X}} \hat{g}_{\text{NTK}}(x)(p - q)(x)dx, \quad (47)$$

then for any $0 < \lambda_{(1)} < 3\sqrt{\nu c_a n}$,

$$\mathbb{P}_{(1)} \left[\hat{C} - \delta_K > 4\lambda_{(1)} \sqrt{\frac{\nu}{c_a n}} \right] \leq 4e^{-\lambda_{(1)}^2/4},$$

and same with $\mathbb{P}_{(1)}[\hat{C} - \delta_K < -4\lambda_{(1)} \sqrt{\frac{\nu}{c_a n}}]$.

Proposition B.2. Suppose $0 < \delta < 1$ and $\sqrt{\log(1/\delta)/(2c_a n)} \leq 0.1\nu$, then under both H_0 and H_1 , there is a good event which happens w.p. $\geq 1 - 4\delta$ over the randomness of \mathcal{D}_{tr} , under which, conditioning on \mathcal{D}_{tr} ,

- (1) Under H_0 , $\mathbb{P}_{(2)}[\hat{T}_a > \hat{C} + 4\lambda \sqrt{\frac{1.1\nu}{c_a n}}] \leq 4e^{-\lambda^2/4}$ if $0 < \lambda < 3\sqrt{1.1\nu c_a n}$;
- (2) Under H_1 , $\mathbb{P}_{(2)}[\hat{T}_a < \hat{C} - 4\lambda \sqrt{\frac{1.1\nu}{c_a n}}] \leq 4e^{-\lambda^2/4}$ if $0 < \lambda < 3\sqrt{1.1\nu c_a n}$.

Proof of Proposition B.2. In this proof we write \hat{g}_{NTK} defined in (46) as \hat{g} for shorthand notation. We have that $\hat{g} = \hat{g}_X - \hat{g}_Y$, where

$$\begin{aligned} \hat{g}_X(x) &:= \int_{\mathcal{X}} K(x, x') \hat{p}_{(1)}(x') dx' = \frac{1}{n_{X,(1)}} \sum_{i=1}^{n_{X,(1)}} K(x, x_i^{(1)}), \\ \hat{g}_Y(x) &:= \int_{\mathcal{X}} K(x, x') \hat{q}_{(1)}(x') dx' = \frac{1}{n_{Y,(1)}} \sum_{i=1}^{n_{Y,(1)}} K(x, y_i^{(1)}), \end{aligned} \quad (48)$$

and both \hat{g}_X and \hat{g}_Y are determined by \mathcal{D}_{tr} . By definition,

$$\begin{aligned} \hat{T}_a &= \int_{\mathcal{X}} (\hat{g}_X - \hat{g}_Y)(x) (\hat{p}_{(2)} - \hat{q}_{(2)})(x) dx \\ &= \frac{1}{n_{X,(2)}} \sum_i \hat{g}_X(x_i^{(2)}) - \frac{1}{n_{Y,(2)}} \sum_i \hat{g}_X(y_i^{(2)}) - \frac{1}{n_{X,(2)}} \sum_i \hat{g}_Y(x_i^{(2)}) + \frac{1}{n_{Y,(2)}} \sum_i \hat{g}_Y(y_i^{(2)}) \\ &:= S_{X,X} - S_{X,Y} - S_{Y,X} + S_{Y,Y}. \end{aligned} \quad (49)$$

Conditioning on a realization of \mathcal{D}_{tr} , due to the independence of \mathcal{D}_{te} from \mathcal{D}_{tr} , the four terms in (49) are independent sums of random variables over the randomness of \mathcal{D}_{te} . Again, we analyze the concentration of these four terms respectively, conditioned on \mathcal{D}_{tr} and we will restrict to good events in $\mathbb{P}_{(1)}$.

We start from $S_{X,X}$. Again by (11), we have $|\hat{g}_X(x)| \leq 1$ for any $x \in \mathcal{X}$. Meanwhile, $\forall x \in \mathcal{X}$,

$$\hat{g}_X(x)^2 = \left(\frac{1}{n_{X,(1)}} \sum_i K(x, x_i^{(1)}) \right)^2 \leq \frac{1}{n_{X,(1)}} \sum_i K(x, x_i^{(1)})^2,$$

and thus, conditioning on \mathcal{D}_{tr} ,

$$\text{Var}_{(2)}(\hat{g}_X(x_i^{(2)})) \leq \mathbb{E}_{x \sim p} \hat{g}_X(x)^2 \leq \frac{1}{n_{X,(1)}} \sum_i \mathbb{E}_{x \sim p} K(x, x_i^{(1)})^2 = \frac{1}{n_{X,(1)}} \sum_i \psi_p(x_i^{(1)}) =: \hat{\nu}_{p,X}, \quad (50)$$

where we define

$$\psi_p(x') := \int_{\mathcal{X}} K(x, x')^2 p(x) dx,$$

and $\hat{\nu}_{p,X}$ is a random variable determined by \mathcal{D}_{tr} . One can verify that by restricting to large probability event in $\mathbb{P}_{(1)}$, $\hat{\nu}_{p,X}$ concentrates at the mean value

$$\mathbb{E}_{(1)}\hat{\nu}_{p,X} = \int_{\mathcal{X}} \psi_p(x')p(x')dx' = \int_{\mathcal{X}} \int_{\mathcal{X}} K(x,x')^2 p(x)dxp(x')dx' = \nu_{p,p} \leq \nu. \quad (51)$$

Specifically, (11) implies that $0 \leq \psi_p(x') \leq 1$, and then by Hoeffding's inequality,

$$\mathbb{P}_{(1)}[\hat{\nu}_{p,X} - \mathbb{E}_{(1)}\hat{\nu}_{p,X} > t] \leq e^{-2n_{X,(1)}t^2} \leq e^{-2c_a n t^2}, \quad \forall t > 0.$$

Let $e^{-2c_a n t^2} = \delta$, where δ is as in the statement of the proposition, then w.p. $\geq 1 - \delta$ in $\mathbb{P}_{(1)}$,

$$\hat{\nu}_{p,X} \leq \mathbb{E}_{(1)}\hat{\nu}_{p,X} + t = \mathbb{E}_{(1)}\hat{\nu}_{p,X} + \sqrt{\frac{\log(1/\delta)}{2c_a n}} \leq \nu + 0.1\nu, \quad (52)$$

and the last inequality is by (51) and the condition of the proposition. We call this good event $E_{X,X}$ in $\mathbb{P}_{(1)}$, under which (52) holds.

Back to $S_{X,X}$, we have that under $E_{X,X}$ in $\mathbb{P}_{(1)}$, and conditioning on the realization of \mathcal{D}_{tr} , $\hat{g}_X(x_i^{(2)})$ as r.v. in $\mathbb{P}_{(2)}$ are bounded as $|\hat{g}_X(x_i^{(2)})| \leq 1$; Meanwhile, by (50) and (52),

$$\text{Var}_{(2)}(\hat{g}_X(x_i^{(2)})) \leq \hat{\nu}_{p,X} \leq 1.1\nu.$$

Then the classical Bernstein gives that $\forall 0 < \lambda < 3\sqrt{1.1\nu n_{X,(2)}}$,

$$\mathbb{P}_{(2)} \left[S_{X,X} - \mathbb{E}_{(2)}S_{X,X} > \lambda \sqrt{\frac{1.1\nu}{n_{X,(2)}}} \right], \mathbb{P}_{(2)} \left[S_{X,X} - \mathbb{E}_{(2)}S_{X,X} < -\lambda \sqrt{\frac{1.1\nu}{n_{X,(2)}}} \right] \leq e^{-\lambda^2/4}.$$

By that $n_{X,(2)} \geq c_a n$, we have that $\forall 0 < \lambda < 3\sqrt{1.1\nu c_a n}$, under the good event $E_{X,X}$ which happens w.p. $\geq 1 - \delta$ in $\mathbb{P}_{(1)}$ and conditioning on \mathcal{D}_{tr} ,

$$\mathbb{P}_{(2)} \left[S_{X,X} - \mathbb{E}_{(2)}S_{X,X} > \lambda \sqrt{\frac{1.1\nu}{c_a n}} \right], \mathbb{P}_{(2)} \left[S_{X,X} - \mathbb{E}_{(2)}S_{X,X} < -\lambda \sqrt{\frac{1.1\nu}{c_a n}} \right] \leq e^{-\lambda^2/4}. \quad (53)$$

Similarly, we can show that, there are good events $E_{X,Y}$, $E_{Y,X}$, and $E_{Y,Y}$ over randomness of \mathcal{D}_{tr} , where each happens in $\mathbb{P}_{(1)}$ w.p. $\geq 1 - \delta$, and under which the similar bound as (53) holds for $S_{X,Y}$, $S_{Y,X}$, and $S_{Y,Y}$ respectively as long as $0 < \lambda < 3\sqrt{1.1\nu c_a n}$. Thus, under the intersection of the four good events, which happens in $\mathbb{P}_{(1)}$ w.p. $\geq 1 - 4\delta$,

$$\mathbb{P}_{(2)} \left[\hat{T}_a - \mathbb{E}_{(2)}\hat{T}_a > 4\lambda \sqrt{\frac{1.1\nu}{c_a n}} \right], \mathbb{P}_{(2)} \left[\hat{T}_a - \mathbb{E}_{(2)}\hat{T}_a < -4\lambda \sqrt{\frac{1.1\nu}{c_a n}} \right] \leq 4e^{-\lambda^2/4}.$$

The above holds under both H_0 and H_1 . Finally, by that $\mathbb{E}_{(2)}\hat{T}_a = \hat{C}$ as defined in (47), this proves parts (1) and (2) of the proposition. \square

Proof of Lemma B.1. Note that \hat{C} is a random variable over the randomness of \mathcal{D}_{tr} only. By definition,

$$\hat{C} = \int_{\mathcal{X}} \int_{\mathcal{X}} K(x,x')(\hat{p}_{(1)} - \hat{q}_{(1)})(x')dx'(p - q)(x)dx = \int_{\mathcal{X}} (\varphi_p - \varphi_q)(x')(\hat{p}_{(1)} - \hat{q}_{(1)})(x')dx',$$

where

$$\varphi_p(x') := \int_{\mathcal{X}} K(x,x')p(x)dx, \quad \varphi_q(x') := \int_{\mathcal{X}} K(x,x')q(x)dx.$$

Because only $n_{X,(1)}$ and $n_{Y,(1)}$ are involved here, in this proof we write $n_{X,(1)}$ as n_X and $n_{Y,(1)}$ as n_Y for notation convenience, and we also denote samples from $X_{(1)}$ and $Y_{(1)}$ by x_i and y_i respectively. By (19), we then have

$$n_X, n_Y \geq c_a n. \quad (54)$$

We then equivalently write \hat{C} as

$$\begin{aligned} \hat{C} &= \frac{1}{n_X} \sum_{i=1}^{n_X} \varphi_p(x_i) - \frac{1}{n_X} \sum_{i=1}^{n_X} \varphi_q(x_i) - \frac{1}{n_Y} \sum_{i=1}^{n_Y} \varphi_p(y_i) + \frac{1}{n_Y} \sum_{i=1}^{n_Y} \varphi_q(y_i) \\ &:= C_{X,X} - C_{X,Y} - C_{Y,X} + C_{Y,Y}, \end{aligned} \quad (55)$$

and we use concentration argument on the four terms respectively.

Due to (11),

$$|\varphi_p(x)| \leq 1, \quad |\varphi_q(x)| \leq 1, \quad \forall x \in \mathcal{X}.$$

Starting from $C_{X,X}$ which is an independent sum of i.i.d. rv's, where $|\varphi_p(x_i)| \leq 1 := L$; By that

$$\varphi_p(x)^2 = \left(\int_{\mathcal{X}} K(x, x') p(x') dx' \right)^2 \leq \left(\int_{\mathcal{X}} K(x, x')^2 p(x') dx' \right) \left(\int_{\mathcal{X}} p(x') dx' \right) = \int_{\mathcal{X}} K(x, x')^2 p(x') dx'$$

we have

$$\text{Var}_{(1)}(\varphi_p(x_i)) \leq \mathbb{E}_{x \sim p} \varphi_p(x)^2 \leq \int_{\mathcal{X}} \int_{\mathcal{X}} K(x, x')^2 p(x') dx' p(x) dx = \nu_{p,p} \leq \nu,$$

where the last inequality is by condition (ii) in Theorem 3.1. The classical Bernstein then gives that $\forall 0 < \lambda < 3\sqrt{\nu n_X}$,

$$\mathbb{P}_{(1)} \left[C_{X,X} - \mathbb{E}_{(1)} C_{X,X} > \lambda \sqrt{\frac{\nu}{n_X}} \right], \mathbb{P}_{(1)} \left[C_{X,X} - \mathbb{E}_{(1)} C_{X,X} < -\lambda \sqrt{\frac{\nu}{n_X}} \right] \leq e^{-\lambda^2/4}.$$

The similar bounds can be derived for $C_{X,Y}$, and for $C_{Y,X}$ and $C_{Y,Y}$ where n_X is replaced with n_Y . By (54), this gives that when $0 < \lambda < 3\sqrt{\nu c_a n} \leq 3\sqrt{\nu n_X}$ and $3\sqrt{\nu n_Y}$,

$$\mathbb{P}_{(1)} \left[\hat{C} - \mathbb{E}_{(1)} \hat{C} > 4\lambda \sqrt{\frac{\nu}{c_a n}} \right], \mathbb{P}_{(1)} \left[\hat{C} - \mathbb{E}_{(1)} \hat{C} < -4\lambda \sqrt{\frac{\nu}{c_a n}} \right] \leq 4e^{-\lambda^2/4}.$$

Observing that $\mathbb{E}_{(1)} \hat{C} = \delta_K$ which is defined in (12) finishes the proof. \square

B.3 Test power of \hat{T}_a with full-bootstrap

We derive here the testing power of the statistic \hat{T}_a computed on split training/testing sets in Subsection 3.2, with a theoretical choice of t_{thres} , similar to as in Theorem 3.1. In practice, the full-bootstrap estimation of t_{thres} can obtain better power than the theoretical one.

Proof of Theorem 3.3. Similar to the proof of Theorem 3.1 by applying Proposition B.3. Due to that the upper bound of \hat{T}_a under H_0 does not have the $\frac{4}{cn}$ term, c.f. Proposition B.3 Part (1) (because the asymmetric kernel MMD is computed from an off-diagonal block of the kernel matrix and the summation in \hat{T}_a does not involve diagonal terms), the value of t_{thres} does not have the $\frac{4}{cn}$ term, and the condition (21) has one term less on the r.h.s. than (15). \square

Proposition B.3 (Concentration of \hat{T}_a). *Assuming (11), (19) and the conditions (i) and (ii) in Theorem 3.1,*

- (1) Under H_0 , when $0 < \lambda < 3\sqrt{c_a \nu n}$, w.p. $\geq 1 - 4e^{-\lambda^2/8}$, $\hat{T}_a \leq 4\lambda \sqrt{\frac{\nu}{c_a n}}$.
- (3) Under H_1 , when $0 < \lambda < 3\sqrt{c_a \nu n}$, w.p. $\geq 1 - 4e^{-\lambda^2/8}$, $\hat{T}_a \geq \delta_K - 4\lambda \sqrt{\frac{\nu}{c_a n}}$.

The proof makes use of the independence of the four datasets $X_{(1)}$, $X_{(2)}$, $Y_{(1)}$ and $Y_{(2)}$, and the concentration of the double summation over the four blocks of the asymmetric kernel matrix.

Proof of Proposition B.3. By definition,

$$\begin{aligned} \hat{T}_a &= \frac{1}{n_{X,(2)}n_{X,(1)}} \sum_{i=1}^{n_{X,(2)}} \sum_{j=1}^{n_{X,(1)}} K(x_i^{(2)}, x_j^{(1)}) - \frac{1}{n_{X,(2)}n_{Y,(1)}} \sum_{i=1}^{n_{X,(2)}} \sum_{j=1}^{n_{Y,(1)}} K(x_i^{(2)}, y_j^{(1)}) \\ &\quad - \frac{1}{n_{Y,(2)}n_{X,(1)}} \sum_{i=1}^{n_{X,(1)}} \sum_{j=1}^{n_{Y,(2)}} K(x_i^{(1)}, y_j^{(2)}) + \frac{1}{n_{Y,(2)}n_{Y,(1)}} \sum_{i=1}^{n_{Y,(2)}} \sum_{j=1}^{n_{Y,(1)}} K(y_i^{(2)}, y_j^{(1)}). \end{aligned} \quad (56)$$

Then, equivalently,

$$\hat{T}_a = T_{X,X} - T_{Y,X} - T_{X,Y} + T_{Y,Y} \quad (57)$$

$$T_{X,X} := \frac{1}{n_{X,(2)}n_{X,(1)}} \sum_{i=1}^{n_{X,(2)}} \sum_{j=1}^{n_{X,(1)}} K(x_i^{(2)}, x_j^{(1)}), \quad T_{Y,X} := \frac{1}{n_{X,(2)}n_{Y,(1)}} \sum_{i=1}^{n_{X,(2)}} \sum_{j=1}^{n_{Y,(1)}} K(x_i^{(2)}, y_j^{(1)}) \quad (58)$$

$$T_{X,Y} := \frac{1}{n_{Y,(2)}n_{X,(1)}} \sum_{i=1}^{n_{X,(1)}} \sum_{j=1}^{n_{Y,(2)}} K(x_i^{(1)}, y_j^{(2)}), \quad T_{Y,Y} := \frac{1}{n_{Y,(2)}n_{Y,(1)}} \sum_{i=1}^{n_{Y,(2)}} \sum_{j=1}^{n_{Y,(1)}} K(y_i^{(2)}, y_j^{(1)}). \quad (59)$$

We analyze the concentration of the four terms respectively, all similarly to the analysis of the “ $\hat{T}_{X,Y}$ ” term in the proof of Proposition B.1, Specifically, for $T_{X,X}$: Define $M := \min\{n_{X,(1)}, n_{X,(2)}\}$, and by (19),

$$M \geq c_a n.$$

By that $\nu_{pp} \leq \nu$ and that the kernel is bounded in absolute value by 1, we have that $\forall 0 < \lambda < 3\sqrt{\nu M}$,

$$\mathbb{P} \left[T_{X,X} - \mathbb{E}_{x \sim p, y \sim p} K(x, y) > \lambda \sqrt{\frac{\nu}{M}} \right], \mathbb{P} \left[T_{X,X} - \mathbb{E}_{x \sim p, y \sim p} K(x, y) < -\lambda \sqrt{\frac{\nu}{M}} \right] \leq e^{-\lambda^2/8},$$

and M can be replaced to be $c_a n$ where the claim remains to hold. Similar bounds hold for $T_{Y,X}$, $T_{X,Y}$, $T_{Y,Y}$, since

$$\min\{n_{X,(1)}, n_{X,(2)}, n_{Y,(1)}, n_{Y,(2)}\} \geq c_n.$$

Putting together, to prove (1) under H_0 , use the concentration bounds for the 4 quantities and under the joint good events, plus that $\text{MMD}_K^2(p, q) = 0$. Part (2) under H_1 is proved similarly. \square

C Experimental details and additional results

C.1 Gaussian mean and covariance shifts

The neural network has 2 fully-connected (fc) layers, i.e. 1 hidden layer, and has the following architecture: the input data dimension $d = 100$, the hidden layer width $m = 512$,

fc (d, m) - softplus - fc ($m, 1$) - loss as in (3)

where (f_{in}, f_{out}) stand for dimensionality of input and output features respectively.

The network mapping $f(x; \theta)$ can be equivalently written as

$$f(x; \theta) = \sum_{k=1}^m a_k \sigma(w_k^T x + b_k), \quad \theta = \{(w_k, b_k, a_k)\}_{k=1}^m. \quad (60)$$

The neural network parameters are initialized such that $a_k \sim \mathcal{N}(0, 1/m)$, $w_k \sim \mathcal{N}(0, I_d)$, and $b_k = 0$. For simplicity, we leave the 2nd layer parameters a_k fixed after initialization and only train the 1st layer parameters w_k and b_k .

Neural network configuration \ width m	256	512	1024
2-layer softplus	82.0	81.6	82.0
2-layer relu	79.8	84.4	82.8
3-layer relu	85.8	88.4	91.0

Table A.1: NTK-MMD with relu activation, different width m , and more layers (to compare to Figure 1, which is computed with 2 fc-layers, softplus activation, width $m=512$). Numbers in the table are testing power (in %).

SGD configuration	Test power of NTK-MMD
Batch-size = 1, epoch= 1 (10)	84.2 (85.0)
Batch-size = 20, epoch= 1 (10)	82.8 (81.6)

Table A.2: NTK-MMD trained with different numbers of epochs and batch sizes. The example of gaussian covariance shift in Section 4.1, $\rho = 0.12$. Test power (in %) with epoch=1 outside brackets, with epoch=10 in brackets.

Remark C.1 (Effective learning rate). The network is trained for 1 epoch (1 pass of the training set) and batch-size 1, using basic SGD. In the notation of Remark 2.2, the theoretical learning rate $\alpha = 0.1$. Note that the definition of loss (3) contains normalization $1/n_X$ and $1/n_Y$, and here $n_{X,(1)} = n_{Y,(1)} = 100$. Comparing to training objective which is usually defined as the summation (with out normalizing by sample size), the effective learning rate here (lr) is $\alpha/100 = 10^{-3}$. Using smaller values of lr produces similar results, but note that reducing lr to be too small may cause numerical issue, due to that the deep learning programs use single precision floating point arithmetic.

The testing powers are approximately computed over n_{run} random replicas. For Figure 1, the most right plot is produced by $n_{\text{run}} = 200$, and all other plots by $n_{\text{run}} = 500$. In the most right plot, $n_{X,(1)} = n_{Y,(1)} = 250$, and the effective lr is $0.1/250 = 4 \times 10^{-4}$.

C.2 Experiments of varying neural network hyperparameters

We conducte additional experiments to investigate the influence of neural network architecture and training hyperparameters.

- Different activation functions, network depths and widths

Table A.1 shows that increasing the network depth can improve testing power, and changing from softplus to relu obtains similar results. We also find in experiments that relu can obtain more robustness of testing power performance with respect to different weight initialization schemes. We observe that the performance with wider networks is generally better, though no longer sensitive beyond a certain m . Theoretically, the convergence to infinite-width limiting NTK may lead to further analysis of the discriminative power of the kernel to distinguish p and q , see the comments in Subsection 4.3.

- General SGD with varying batch-size, epochs, and batch-size

Theoretically, the analysis covers general SGD (more than one epoch and different batch size): The proof in Appendix A.2 generalizes to such cases because the residual error of the Taylor expansion of the network mapping $f(x; \theta)$ still applies.

Empirically, we verify that the testing power of NTK-MMD is not sensitive to batch size nor a few more epochs, as illustrated in Table A.2. This agrees with the theory that \hat{T}_{net} computed with different batch-size and small number of epochs all approximate the exact NTK-MMD at time zero. In other experiments in the paper, we focus on batch-size =1 to show that NTK-MMD allows extremely small batch-size. Note that the advantage of NTK-MMD is particularly pronounced in the one-pass training, i.e., we can only visit the data in one-pass, which commonly appears in the streaming data setting.

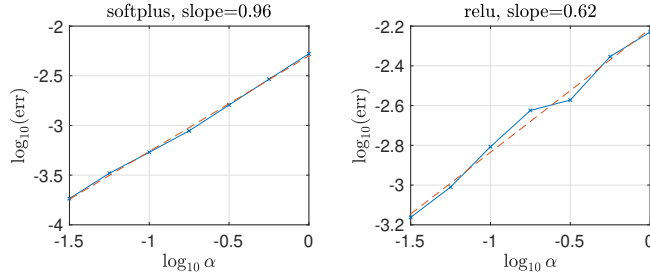


Figure A.1: Numerical computation of the (relative) approximation error $\text{err} = |\hat{T}_{\text{net}}(t) - \hat{T}_{\text{NTK}}|/|\hat{T}_{\text{NTK}}|$. The network has 2-fc layers with softplus (or relu) activation and width $m = 512$, and the simulated data distribution is Gaussian covariance shift in dimension 100.

C.3 Computation of the exact NTK MMD

The neural network setting is the same as in Subsection 4.1, and here we derive the expression of the NTK kernel at $t = 0$, which was used to compute the “ntk1” and “ntk2” statistics.

For the network function as in (60),

$$K_0(x, x') = \left(\sum_{k=1}^m a_k^2 \sigma'(w_k^T x + b_k) \sigma'(w_k^T x' + b_k) \right) (1 + x^T x'), \quad (61)$$

where $\sigma(z) = \log(1 + e^z)$ is the softplus function, and is differentiable on \mathbb{R} . Thus the kernel for any pair of samples x and x' is analytically computable once the network parameters are initialized. In our experiments, we compute $K_0(x, x')$ as in (61) with finite hidden-layer width m and given realizations of the $t = 0$ network parameters.

C.4 Comparison to neural network classification tests

The network is fc 3-layer with relu activation and width $m = 512$. Two C2ST baselines are trained with Adam and SGD respectively, and trained for 1 and 10 epochs. (By SGD, we mean vanilla SGD with constant step-size and no momentum.) NTK-MMD uses SGD, epoch = 1. We also experiment under H_0 to verify that the Type-I error achieves $\alpha_{\text{level}} = 0.05$.

Since [36] already compared C2ST’s with optimization-based linear time kernel tests, namely ME and SCF tests [14, 29] and showed that C2ST’s are generally better, we cite the results therein for comparison.

C.5 MNIST distribution abundance change

The neural network has two convolutional (conv) layers:

- conv 5x5x1x16 - relu - maxpooling 2x2
- conv 5x5x16x32 - relu - maxpooling 2x2
- fc (·, 128) - relu - fc (128, 1) - loss

where the dimension of f_{in} in the 1st fc layer is by flattening the input feature, which gives $f_{in} = 4^2 \cdot 32$ in this case.

In the online training of the network, we use batch size = 1, theoretical lr $\alpha = 0.01$, and SGD with momentum 0.9. Adding momentum to SGD is common in neural network practice, and we adopt it here as to examine the behavior of the model: theoretically, under the NTK assumption, we expect similar behavior with and without momentum in short-time training with SGD. As has been explained in Appendix C.1, by that $n_{X,(1)} = n_{Y,(1)} = 10^3$, the effective lr is $\alpha/10^3 = 10^{-5}$.

Test statistics \ n_{tr}	100	200	300	500	1000	2000
<i>gmmd</i>	62.0	93.2	99.6	-	-	-
<i>gmmd-lin</i>	7.0	10.8	12.6	16.0	24.4	36.4
NTK-MMD	35.4	67.6	86.2	98.2	100.0	100.0

Table A.3: Testing power (in %) of MNIST density departure example in Subsection 4.4. *gmmd* is Gaussian kernel MMD, and *gmmd-lin* the linear-time version. Results of *gmmd* for n_{tr} greater than 300 are omitted due to slow computation.

C.6 Human activity change-point detection

The (MSRC-12) Kinect gesture dataset consists of sequences of human skeletal body part movements (represented as body part locations) collected from 30 people performing 12 gestures. There are 18 sensors in total, and each sensor records the coordinates in the three-dimensional Cartesian coordinate system at each time.

The net MMD statistic is computed using a 2-layer fc network having 512 hidden nodes and softplus activation. We use effective lr 0.0015 and SGD with momentum 0.9 in the one-pass training with batch-size one.

C.7 Comparison to linear time MMD

The test power comparison of NTK-MMD, Gaussian kernel MMD and the linear-time version as in [23, Section 6], on the example of MNIST data in Section 4.4 is given in Table A.3. On the examples in Section 4.1 (Figure 1) linear-time gaussian MMD baseline gives inferior power (all less than 10%, details omitted). This version of linear-time MMD only provides a global test statistic but not directly a witness function (to indicate where p and q differ), while NTK-MMD training obtains network witness function which approximates the kernel witness function of NTK.

As alternative linear-time MMD tests, the ME and SCF tests [14, 29] involve additional gradient-based optimization of model parameters and may not have optimization convergence guarantee for general data distributions. NTK-MMD has comparable computational and memory complexity to classification neural network tests (the order is the same, but only one epoch is needed and batch size can be as small as one), and has learning guarantee via NTK approximation as shown in Section 2.3 and Section 3.